

A TWO-DIMENSIONAL STOCHASTIC MODEL FOR PREDICTION OF  
LOCALIZED CORROSION

A thesis presented to  
the faculty of the  
Russ College of Engineering and Technology of Ohio University

In partial fulfillment  
of the requirements for the degree  
Master of Science

Ying Xiao  
November 2004

This thesis entitled  
A TWO-DIMENSIONAL STOCHASTIC MODEL FOR PREDICTION OF  
LOCALIZED CORROSION

by  
Ying Xiao

has been approved for  
the Department of Chemical Engineering  
and the Russ College of Engineering and Technology by

Srdjan Nesic  
Professor of Chemical Engineering

Dennis Irwin  
Dean, Russ College of Engineering and Technology

XIAO, YING. M.S. November 2004. CHEMICAL ENGINEERING

A TWO-DIMENSIONAL STOCHASTIC MODEL FOR PREDICTION OF  
LOCALIZED CORROSION (71pp)

Director of Thesis: Srdjan Nesic

The two-dimensional (2-D) stochastic model, which describes the balance of two processes: corrosion (leading to metal loss) and precipitation (leading to metal protection), is able to predict localized corrosion, which is the most serious type of corrosion attack found in practice. The model uses uniform corrosion rate and surface-scaling tendency predicted by a 1-D mechanistic corrosion model as the inputs and can predict the possibility of localized corrosion as a function of primitive parameters such as temperature, pH, partial pressure of CO<sub>2</sub>, velocity, etc. The maximum penetration rate as well as uniform corrosion rate can be predicted and used to describe the severity of the localized attack.

Approved:

Srdjan Nesic

Professor of Chemical Engineering

## ACKNOWLEDGEMENTS

I want to thank all the individuals who helped me complete this thesis. Although I cannot list them all within this small page, I do want to express my deepest gratitude to some of them directly involved in my research.

I would like to sincerely thank my advisor, Prof. Srdjan Nestic, for his guidance, support and encouragement. His insight and knowledge in corrosion were the greatest benefits to this work.

Many sincere thanks are due to my thesis committee members, Professor Daniel Gulino, and Professor Dusan Sormaz, for their time, instructions, and patience during my research.

I am pleased to acknowledge the support from Dr. Bert. M. Pots, for his sharing the initial idea of this project and help to publish the work at NACE.

I am also greatly thankful to Mr. Herold for his instructions when I was writing my thesis. This thesis could not be finished without his knowledge, and support.

Finally, special thanks to my husband, Dong Liu, my parents and sister for their support and encouragement all of these years.

## TABLE OF CONTENTS

Page	
Abstract.....	3
Acknowledgements.....	4
List of Tables.....	7
List of Figures.....	8
Chapter 1. Introduction.....	11
Chapter 2. Literature Review.....	15
2.1 CO <sub>2</sub> Corrosion.....	15
2.2 Enviromental Factors.....	17
2.2.1. Temperature.....	18
2.2.2. pH.....	19
2.2.3. Pressure.....	20
2.2.4. Flow .....	21
2.3 Film Formation and Its Influencing Factors.....	21
2.4 Research Work on Localized Corrosion.....	23
2.5 Localized Corrosion Model.....	25
Chapter 3. Model Development.....	35
3.1. Modification of the Corrosion Rule.....	36
3.2. Modification of Precipitation Rule.....	37
3.3. Link to OU 1-D Mechanistic Model.....	41
3.4. Film Growth Algorithm.....	46

3.5. Implement a Path-Searching Algorithm to Remove Isolated Islands.....	51
3.6. Localized Corrosion Tendency.....	55
Chapter 4. Verification.....	56
4.1 Comparison.....	56
4.2. Parameter Study.....	59
Chapter 5. Conclusions.....	64
Chapter 6. Future Work.....	65
References.....	66

LIST OF TABLES

Table	Page
3.1. Test Matrix.....	44

## LIST OF FIGURES

Figure	Page
Figure 1.1. Summary of natural gas transmission pipeline incidents by cause .....	11
Figure 1.2. Corrosion accident categories in a major industry .....	13
Figure 2.1. The effect of pH on the solubility of iron carbonate at 2 bar pCO <sub>2</sub> , 40°C .....	20
Figure 2.2. Two samples of simulated metal surface morphology following rapid uniform corrosion without any film precipitation .....	28
Figure 2.3. Two samples of the simulated metal surface morphology following rapid precipitation, which leads to a protective film and very little corrosion. ....	29
Figure 2.4. Two samples of simulated metal surface morphology following slow precipitation leading to an unprotective film and a moderate corrosion rate.....	30
Figure 2.5. Two samples of simulated metal surface morphology following moderate precipitation leading to a partially protective film and localized corrosion...	31
Figure 3.1. Surface morphology prediction taken from the study of 2-D localized corrosion model by Netic, Xiao, and Pots [2004].....	40
Figure 3.2. SEM images of the corroded steel surfaces taken from the study of CO <sub>2</sub> corrosion in multiphase flow taken from the study by Netic and Lunde [1994].....	40
Figure 3.3. Predictions for the case of a 1%NaCl solution, at T = 80°C, pCO <sub>2</sub> = 0.52bar, P <sub>total</sub> = 1bar, C <sub>Fe<sup>2+</sup></sub> = 100ppm., v=1 m/s.....	45
Figure 3.4 Film morphology taken from the proposed 2-D Model.....	48
Figure 3.5 Film morphology and cross section of iron carbonate at pH 6.6, 80°C, 50ppm C <sub>Fe<sup>2+</sup></sub> , stagnant flow.....	48
Figure 3.6 Comparison of the film morphology before (top) and after (bottom) using a random film formation algorithm at pH 6.6, 80°C, 5ppm Fe <sup>2+</sup> and 0.52bar pCO <sub>2</sub> .....	49

Figure 3.7 Comparison of the film morphology at higher magnification before (top) and after (bottom) using a random film formation algorithm at pH 6.6, 80°C, 5ppm Fe <sup>2+</sup> and 0.52bar p <sub>CO2</sub> .....	50
Figure 3.8 Comparison of the film morphology before (top) and after (bottom) using a random film formation algorithm at pH 6.5, 80°C, 50ppm Fe <sup>2+</sup> and 0.52bar p <sub>CO2</sub> .....	51
Figure 3.9 Image for isolated islands taken from original Pots' algorithm at ST=0.31.....	52
Figure 3.10. Comparison of the surface morphology, uniform corrosion rate and maximum penetration rate before (bottom) and after (top) implementing path-searching algorithm at pH 6.26, 80°C, 50ppm Fe <sup>2+</sup> and 0.52bar p <sub>CO2</sub> .....	53
Figure 3.11. Comparison of the surface morphology, uniform corrosion rate and maximum penetration rate before (bottom) and after (top) implementing path-searching algorithm at pH 6.0, 80°C, 50ppm Fe <sup>2+</sup> and 0.52bar p <sub>CO2</sub> .....	54
Figure 3.12. Comparison of the surface morphology, uniform corrosion rate and maximum penetration rate before (bottom) and after (top) implementing path-searching algorithm at pH 6.6, 80°C, 50ppm Fe <sup>2+</sup> and 0.52bar p <sub>CO2</sub> .....	54
Figure 4.1. Comparison of uniform corrosion rate between 2-D prediction, 1-D prediction and experimental at pH 6.0, 80°C, 0.52bar p <sub>CO2</sub> , 50ppm Fe <sup>2+</sup> , rpm=0.....	57
Figure 4.2. Comparison of film morphology between 2-D prediction, 1-D prediction and experimental at pH 6.0, 80°C, 0.52bar p <sub>CO2</sub> , 50ppm Fe <sup>2+</sup> , rpm=0.....	57
Figure 4.3. Comparison of uniform corrosion rate between 2-D prediction, 1-D prediction and experimental at pH 6.3, 80°C, 0.52bar p <sub>CO2</sub> , 50ppm Fe <sup>2+</sup> , rpm=0.....	58
Figure 4.4. Comparison of film morphology between 2-D prediction, 1-D prediction and experimental at pH 6.3, 80°C, 0.52bar p <sub>CO2</sub> , 50ppm Fe <sup>2+</sup> , rpm=0.....	58
Figure 4.5. Comparison of uniform corrosion rate between 2-D prediction, 1-D prediction and experimental at pH 6.6, 80oC, 0.52bar p <sub>CO2</sub> , 50ppm Fe <sup>2+</sup> ,rpm=0.....	59
Figure 4.6. Comparison of film morphology between 2-D prediction, 1-D prediction and experimental at pH 6.6, 80oC, 0.52bar p <sub>CO2</sub> , 50ppm Fe <sup>2+</sup> , rpm=0.....	59

Figure 4.7 Film morphology and corresponding corrosion rate predicted by 2-D model at 0.54bar $p_{CO_2}$ , 0ppm $Fe^{2+}$ , 80 °C, pH 6.6,1m/s.....	61
Figure 4.8 Film morphology and corresponding corrosion rate predicted by 2-D model at 0.54bar $p_{CO_2}$ , 5ppm $Fe^{2+}$ , 80 °C, pH 6.6,1m/s.....	61
Figure 4.9 Film morphology and corresponding corrosion rate predicted by 2-D model at 0.54bar $p_{CO_2}$ , 10ppm $Fe^{2+}$ , 80 °C, pH 6.6,1m/s.....	61
Figure 4.10 Film morphology and corresponding corrosion rate predicted by 2-D model at 0.54bar $p_{CO_2}$ , 25ppm $Fe^{2+}$ , 80 °C, pH 6.6, 1m/s.....	62
Figure 4.11 Film morphology and corresponding corrosion rate predicted by 2-D model at 0.54bar $p_{CO_2}$ , 28ppm $Fe^{2+}$ , 80 °C, pH 6.6,1m/s.....	62
Figure 4.12 Film morphology and corresponding corrosion rate predicted by 2-D model at 0.54bar $p_{CO_2}$ , 30ppm $Fe^{2+}$ , 80 °C, pH 6.6, 1m/s.....	63
Figure 4.13 Film morphology and corresponding corrosion rate predicted by 2-D model at 0.54bar $p_{CO_2}$ , 50ppm $Fe^{2+}$ , 80 °C, pH 6.6, 1m/s.....	63

CHAPTER 1  
INTRODUCTION

Carbon and low alloy steel are the principal construction materials for natural gas pipelines due to their advantages in economy, availability and strength. It is estimated that carbon and low alloy steel comprise 99% of materials used in the oil industry. Although there have been many developments in corrosion resistant alloys over the past few decades, carbon and low alloy steel are the most cost effective options. Usually these materials are three to five times cheaper than stainless steel.

Natural Gas Transmission Pipeline Incident Summary by Cause 1/1/2002 - 12/31/2003						
Reported Cause	Number of Incidents	% of Total Incidents	Property Damages	% of Total Damages	Fatalities	Injuries
Excavation Damage	32	17.8	\$4,583,379	6.9	2	3
Natural Force Damage	12	6.7	\$8,278,011	12.5	0	0
Other Outside Force Damage	16	8.9	\$4,688,717	7.1	0	3
Corrosion	46	25.6	\$24,273,051	36.6	0	0
Equipment	12	6.7	\$5,337,364	8.0	0	5
Materials	36	20.0	\$12,130,558	18.3	0	0
Operation	6	3.3	\$2,286,455	3.4	0	2
Other	20	11.1	\$4,773,647	7.2	0	0
<b>Total</b>	<b>180</b>		<b>\$66,351,182</b>		<b>2</b>	<b>13</b>

Figure 1.1. Summary of natural gas transmission pipeline incidents by cause [U.S Transportation Department, 2004]

Natural gas pipeline failures are very costly due to production losses, repair costs, and personnel and environmental damages. Figure 1. lists the summary of natural gas transmission pipeline incidents by cause in 2002 and 2003, as reported by the U. S.

Department of Transportation Research and Special Programs Administration, Office of Pipeline Safety (RSPA/OPS) [U.S Transportation Department, 2004]. It demonstrates that corrosion (internal and external) is the most common cause of natural gas transmission pipeline incidents, accounting for around 25% of all the incidents in 2002-2003. In certain circumstances, internal corrosion comprises almost 50% of all incidents (Alberta 1998).

Low-alloy steel pipeline carrying natural gas from well heads to treatment units can be subject to corrosion caused by carbonic acid formed from carbon dioxide and water often present as impurities in the produced streams. Carbon dioxide corrosion, also called “sweet corrosion”, is by far the most prevalent form of internal corrosion encountered in oil and gas production. It is getting more and more attention in recent years with the fast development of modern oil and sweet gas recovery techniques.

The internal corrosion failures are generally not caused by uniform corrosion, but rather by localized corrosion such as pitting and/or flow induced localized corrosion (FILC). In order to run the oil and gas pipelines under safe and reliable conditions, it is important to predict the amount of internal corrosion that occurs before significant damage occurs. When it comes to monitoring, a number of electrochemical apparatus are qualified to test the uniform corrosion; however there is not much progress in monitoring localized corrosion. So, in practice, localized corrosion is the most serious and frequent cause of pipeline failure. The following pie chart in Figure 1. summarizes the findings of 363 corrosion failure cases investigated in a major chemical processing company.

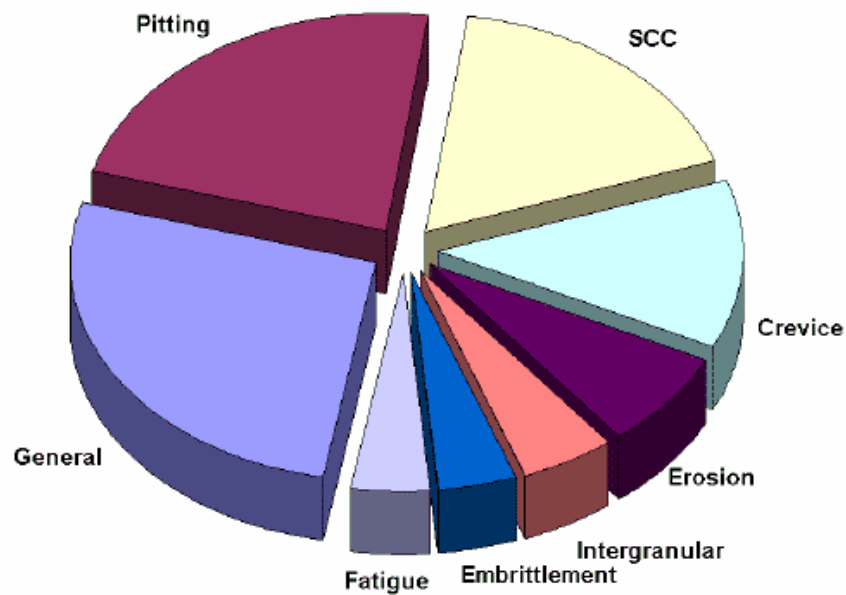


Figure 1.2 Corrosion accident categories in a major industry

The percentage of accidents, caused by the two types of localized corrosion, pitting and crevice corrosion, is 22% and 12%, respectively. Stress corrosion cracking (SCC), which is often initiated by pitting, accounts for 18%. So, the failures directly caused by localized corrosion comprise 50% of the total accident. Currently, few effective techniques are available for monitoring localized corrosion in an oilfield [Fu 1996]. Nearly all the generally used electrochemical techniques have some shortcomings when detecting localized corrosion.

Due to the difficulty of monitoring localized attack, in this thesis, a stochastic localized corrosion model considering film formation is proposed to predict the occurrence of localized corrosion. The model has been calibrated with reliable experimental data and its objective is to assist in safe pipeline design and/or operation.

## CHAPTER 2

### LITERATURE REVIEW

The corrosion process is a physicochemical process, and the mechanism of carbon steel corrosion in CO<sub>2</sub> environment is extremely complex. Depending upon the system conditions, either uniform or localized corrosion occurs. In recent decades, significant attention has been paid to uniform corrosion and the mechanism of CO<sub>2</sub> corrosion. Some uniform corrosion models have been developed [Nordsveen 2003 and de Waard 1995]. However, relatively little attention has been given to localized corrosion. It is still not well understood. A lot of research effort is needed before a full mechanism of localized corrosion model is established.

#### 2.1 CO<sub>2</sub> Corrosion

A number of studies have been done under varying conditions of pressure, temperature, pH value and water cut considering CO<sub>2</sub> corrosion. The basic CO<sub>2</sub> corrosion reactions have been clearly understood and well accepted based on the work in the recent decades. The major chemical reactions, include CO<sub>2</sub> dissolution and hydration to form a weak carbonic acid, are described as follows:



Then it dissociates into bicarbonate and carbonate ions through two steps:



When the concentrations of  $Fe^{2+}$  and  $CO_3^{2-}$  ions exceed the solubility limit ( $K_{sp}$ ), they combine with each other to form solid iron carbonate film (also called corrosion product film) as follows:

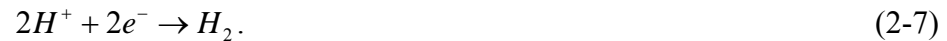


Here  $K_{sp}$  is a function of temperature and ionic strength.  $CO_2$  corrosion rates can be reduced significantly when iron carbonate film precipitates on the surface of the steel.

The electrochemical reactions on the steel surface include the anodic reaction of iron dissolution:



and two cathodic reactions. One of the reactions is the hydrogen evolution reaction:



the other is direct reduction of carbonic acid:



## 2.2 Environmental Factors

Considering the basic reactions in CO<sub>2</sub> corrosion shown above, one can appreciate that a number of environmental factors, such as solution chemistry, flow velocity, temperature, pressure, and pH value etc., can affect the uniform CO<sub>2</sub> corrosion rate of mild steel. Significant progress in recognition of the major parameters influencing phenomenology and kinetics of the uniform corrosion of various steels in CO<sub>2</sub> has been achieved. But there still is no understanding of the exact mechanisms of processes leading to the localized corrosion. Brossia [2000] suggested that the ratio of the chloride concentration to the total carbonate concentration, solution pH, and solution temperature, play critical roles in establishing conditions that promote localized corrosion, as well as in influencing the rate of propagation at potentials above repassivation potential. He concluded that there is no clear dependency of the severity or mode of attack on each independent parameter and the initiation of pit seem to be of stochastic nature.

The oil industry's experience with deep gas wells indicates that corrosion is not severe at places where scale uniformly covers the surface of the tubing. Laboratory tests have repeatedly demonstrated that a thin adherent layer of ferrous carbonate deposited on the surface of a corroding material significantly reduces the corrosion rate. So, any changes in the parameters that can increase precipitation kinetics (e.g. increasing iron concentration, carbonate concentration, or temperature) might improve film adherence under this scenario [Johnson 1991]. Corrosion rate is thus decreased by such strategies.

The effect of the most important factors on CO<sub>2</sub> corrosion are temperature, pH value, pressure, solution composition, and flow, and each will be discussed separately.

### 2.2.1 Temperature

Temperature has major effects on corrosion. On one hand, higher temperature increases reaction rates and transport of species, and hence results in a higher corrosion rate. On the other hand, the increased temperature also accelerates the kinetics of corrosion product precipitation. In CO<sub>2</sub> solutions, the corrosion product, iron carbonate precipitates and deposits on the metal surface after its solubility limit is reached. The rate of ferrous carbonate precipitation is extremely temperature sensitive [Johnson 1991]. According to Johnson, at low temperatures, precipitation progresses more slowly than corrosion reactions. At elevated temperatures, transport limited ferrous carbonate deposition is theoretically limited by the corrosion reaction. Corroding surfaces may be immediately passivated by FeCO<sub>3</sub> precipitation at high temperature. At intermediate temperatures, ferrous carbonate may drive the corrosion reaction by removing iron from solution at approximately the same rate as it is provided by corrosion.

Dugstad *et al.* [1994] reported that increased corrosion rates with increasing temperature in a single-phase flow reached a maximum corrosion rate between 60°C and 90°C. However, there is no research that reveals the effect of temperature on localized corrosion.

### 2.2.2 pH

Since pH value indicates the concentration of protons in solution, which is one of the major species involved in cathodic reaction of corrosion process, pH value of the solution has been shown to play a dominant role in determining the corrosion mode of carbon steels. High pH value decreases the  $H^+$  reduction rate of cathodic reaction due to the insufficient protons in the solution, while low pH value enhances it. A correlation between pH value and cathodic corrosion rate has been reported as

$$\log i_c = -A pH + B \quad (2-9)$$

where  $i_c$  is the corrosion current,  $A$  is a positive number and  $B$  is a constant. Different cathodic mechanism gave different  $A$  values [de Waard 1975, Netic 1996].

In addition to the effects on the electrochemical reaction rates, pH value also has a dominant effect on the formation of iron carbonate films due to its effect on the solubility of iron carbonate, as illustrated in Figure 2.1.

The figure shows that solubility of iron carbonate is reduced with the increase of pH under this condition. Thus, if all the other conditions stay the same, a higher pH value results in an increased saturation of iron carbonate. If the concentration of iron concentration exceeds the saturation limit, iron carbonate scale forms and continuously decreases the corrosion rate.

So, higher pH value decreases corrosion rate by reducing cathodic reaction and forming scales.

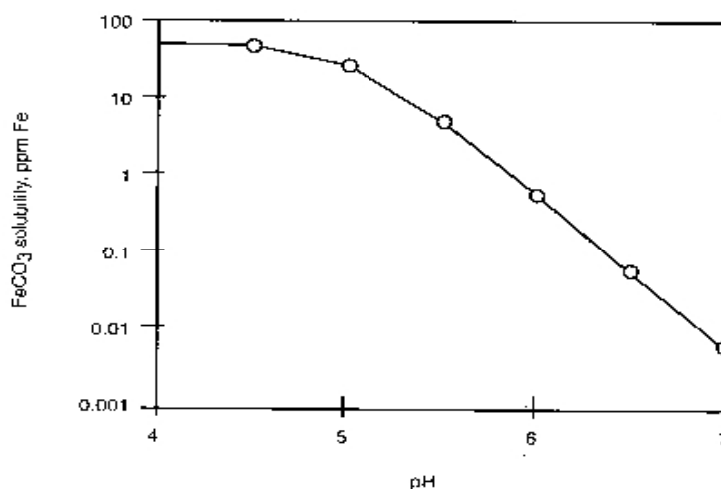


Figure 2.1 The effect of pH on the solubility of iron carbonate at 2 bar  $p_{\text{CO}_2}$ , 40°C [Dugstad, 1992].

### 2.2.3 Pressure

The total pressure in the system usually only changes some fluid properties such as the gas density and viscosity. However, the partial pressure of  $\text{CO}_2$  (or, the fugacity of  $\text{CO}_2$  under extreme high pressure) is a major concern due to high solubility of  $\text{CO}_2$  in aqueous water. Generally speaking, an increase in  $\text{CO}_2$  partial pressure will lead to an increase in corrosion rate. However, increased  $\text{CO}_2$  partial pressure could increase the  $\text{CO}_3^{2-}$  concentration in the system when the condition is favorable for formation of iron carbonate film. Thus, the actual corrosion rate may differ when compared to film-free corrosion [Nesic et al., 2002].

### **2.2.4 Flow**

Corrosion caused by fluid flow is usually called flow affected or flow accelerated corrosion (FAC). Flow affects corrosion mainly through the mass transport process involved in the corrosion mechanism. Generally speaking, higher flow rates are directly associated with higher turbulence and more thorough mixing in the solution. It affects not only the corrosion rate, but also the precipitation rate of iron carbonate [Nesic et al., 2002] by bring more corrosive species onto the steel surface and corrosion products away from the steel surface. Both effects contribute to less protective films being formed at higher velocities. With extremely high velocities, flow can even mechanically remove corrosion product films and can cause FILC, which is also called erosion corrosion.

Flow regime could be a very important factor for corrosion when multiphase flow exists. Water being in contact with the steel surface is a prerequisite for CO<sub>2</sub> corrosion. For some flow regime, such as stratified or annular flow regime, water spreads on the steel surface and causes corrosion. However, for some other flow regime, such as slug flow regime, water could be all picked up by oil/gas and hence results in a low corrosion rate. The severity of the CO<sub>2</sub> corrosion attack is proportional to the time that the steel surface is wetted by the water phase [Kermani and Smith, 1997]. The effect of the flow regime can not be separated from the water/oil/gas ratio.

### **2.3 Film Formation and Its Influencing Factors**

As we know, corrosion is usually not severe in the place where forms scale. Laboratory tests illustrate that the major composition of the scale in CO<sub>2</sub> corrosion is iron

carbonate. The protective property of iron carbonate was obtained by offering greater resistance to diffusion of species involved in the electrochemical reactions and/or by simply blocking the reaction surface [Nesic and Lunde, 1994].

The precipitation kinetics of iron carbonate proposed by van Hunnik et al. [1996] is as follows:

$$[Fe^{2+}]_{prec} = k_r \frac{A}{V} K_{sp} (S - 1)(1 - S^{-1}) \quad (2-10)$$

where  $k_r$  is a temperature-dependent rate constant,  $A/V$  is the ratio of metal surface area to solution volume, and  $S$  is defined as

$$S = \frac{[Fe^{2+}][CO_3^{2-}]}{K_{sp}} \quad (2-11)$$

Here  $K_{sp}$  is the solubility product of iron carbonate, which is a function of temperature and solution ionic strength. Variables  $[Fe^{2+}]$  and  $[CO_3^{2-}]$  represent the equilibrium concentrations of the solution.

According to (2-11), any changes of the parameters that increase precipitation kinetics might improve film protectiveness [Johnson 1991], and hence decrease corrosion rate. Protective iron carbonate films have been observed in systems with high  $Fe^{2+}$  concentrations, high  $P_{CO_2}$ , and high pH, which all lead to high  $S$ , and at high temperature, which lead to high  $k_r$  [Nesic 2003].

The protectiveness of the scale is not only related to the precipitation kinetics, but also related to the scale morphologies. Experimental data demonstrated [De Moraes et al. 2000] that a thin (less than 30  $\mu\text{m}$ ), compact and adherent layer of iron carbonate deposited onto the surface of a corroding material significantly reduces the corrosion rate when comparing to a thick ( $\sim 100$   $\mu\text{m}$ ) and porous scale. This highly protective scale was present only with high temperature (93°C) and high pH (pH>5.0).

van Hunnik et al. [1996] proposed a so-called “scaling tendency” concept to describe the protectiveness of the film. The scaling tendency is defined as the ratio of the scale precipitation rate to the corrosion rate expressed in the same units. Obviously, when  $ST \ll 1$ , the rapidly corroding metal surface opens voids under the film much faster than precipitation can fill them out, which leads to porous and unprotective films. For instance, at room temperature, little or no iron carbonate film forms even at high super saturations as a result of the slow kinetics of the precipitation reaction. This effect is also attributable to the fact that the metal surface “corrodes away” under the film. As  $ST$  exceeds 0.5, conditions become favorable for formation of dense protective iron carbonate films.

## **2.4 Research Work on Localized Corrosion**

Localized corrosion is the type of corrosion where an intense attack occurs at localized sites on the metal surface while the rest of the surface corrodes at a much lower rate, either because of an inherent property of the component material or because of some environmental effect. For instance, if corrosion protection breaks down locally then corrosion may be initiated at these local sites. Under such circumstances, it has been

shown that the anodic surface area ( $S_a$ ), where  $Fe$  will release its two electrons and become  $Fe^{2+}$ , is much smaller than the cathodic surface area ( $S_c$ ), where the positive  $H^+$  ions usually will gain the electrons and become a  $H_2$ . The small ratio of  $S_a/S_c$  can drive corrosion to a higher rate by  $Fe$  trying to release sufficient electrons to be consumed at the cathodic surface.

Some progress has been achieved in the recognition of major parameters influencing phenomenology and kinetics of the uniform corrosion. But there is yet no full understanding of the exact mechanisms of the processes leading to localized corrosion.

Flow induced localized corrosion (FILC) is a typical kind of localized corrosion. Joosten [1994] initiated the experiments to observe and record the development of the corrosion process under flowing conditions. His experiments laid a foundation for the understanding of localized corrosion. The most common FILC is mesa attack. Nyborg [1998] investigated initiation and growth of mesa attack by video recordings in flow loop experiments performed at  $80^\circ C$  and a pH value of 5.8. It is then proposed that a partially protective corrosion film is a prerequisite for mesa attack.

Although flow is a crucial parameter to initiate localized corrosion, it is well known that there are other environmental factors, such as pH, temperature, partial pressure of  $CO_2$ ,  $Cl^-$  concentration, material compositions, etc [Sun 2003] that cause carbon steel to undergo a rapid localized corrosion process. Brossia [2000] studies some parameters that influence the rate of propagation of pitting and he didn't find a clear dependency of the severity or mode of attack on each individual parameter. But he concluded that the initiation of pit seems to have a stochastic nature.

Sun and Netic [2003] studied a number of factors that might influence localized corrosion in wet gas flow, including pH, temperature, pressure, flow velocity, flow regime, water cut and steel type. These studies confirmed Nyborg's assumption that partially protective film is a prerequisite for localized attack.

## **2.5 Localized corrosion model**

Significant progress has been achieved in understanding uniform CO<sub>2</sub> corrosion, and hence some uniform corrosion models have been built successfully. However, far less attention has been given to localized CO<sub>2</sub> corrosion. It is not well understood yet, and it is more difficult to predict or detect localized corrosion than uniform corrosion.

A FILC prediction model was proposed by Gunaltun [1996]. He applied a turbulence factor to the general corrosion rate assuming the flow as being the main parameter initiating localized attack.

In 1999, Schmitt developed a model for the prediction of flow induced localized corrosion [1999]. The model correlates the hydrodynamic forces exerted onto corrosion product scales with the fracture stress of the scales. The model is based on the assumption that turbulence elements in the near-wall region of the turbulent boundary layer exchange momentum with the wall and fatigue the corrosion product scale above critical wall shear stresses [Schmitt 2000]. The author also claims that extrinsic stresses such as wall shear stresses in flowing media are generally too small to contribute much to the local destruction of scales [Schmitt 1996].

Although flow is a very important factor to induce localized corrosion, it has been proved that other parameters such as pH value, temperature, partial pressure of CO<sub>2</sub>, and solution chemistry, can also induce and/or propagate localized corrosion. So, in this thesis, a model taking into account all of these factors is proposed.

Localized corrosion of metals is a random process in nature [Williams 1984 and 1985, Wu 1997]. It is believed to be related to two random processes: the breakdown of the passive film and the repassivation of the exposed area [Bertocci 1986, Hashimoto 1992, Stockert 1989, Pistdrius 1992, Gabrielli 1990, and Gabrielli 1992]. The probabilistic character of localized attack makes a stochastic approach possible [Williams 1984 and 1985, Wu 1997]. The random (stochastic) process exhibits marked deterministic features to form stable pitting due to the statistical results of a large number of performances of these two processes [Hoerle 1998].

In 1996, Pots [van Hunnik and Pots 1996] wrote a two-dimensional (2-D) stochastic algorithm to simulate the morphology of localized attack. The rule-based algorithm is based on the assumption that the morphology of corrosion attack depends on the balance of two processes: corrosion (leading to metal loss) and precipitation (leading to metal protection). This balance has effectively been quantified by van Hunnik *et al.* [1996] using a single parameter, the scaling tendency (ST),

$$ST = \frac{R_{FeCO_3}}{CR} \quad (2-12)$$

where  $R_{FeCO_3}$  is the precipitation rate of iron carbonate and  $CR$  the corrosion rate. Both are expressed in the same volumetric (e.g. mm/y) units. It has been experimentally observed that if the precipitation rate overwhelms the corrosion rate, a protective film forms onto the metal surface and the corrosion rate is greatly reduced. Correspondingly, if the corrosion rate is much larger than the precipitation rate, protective films cannot be formed since corrosion creates voids underneath the film faster than precipitation can fill them up. According to a recent experimental study by Sun and Netic [2003], there is a “gray zone” between these extremes where localized corrosion occurs and the corresponding scaling tendency is between 1 and 3.

For the original Pots’s [1996] algorithm,  $ST$  ( $ST$  has been defined above) is used as the unique input parameter describing the corrosion process. For example, when  $ST$  is set to zero (that is, there is no film precipitation), the algorithm predicts uniform corrosion with a constant metal maximum penetration rate as shown in Figure 2.. On the other extreme, when the input  $ST$  is set to 1 (1 represents the largest value allowed in the algorithm), a protective film is formed very fast, thus hindering any further corrosion, as shown in Figure 2..

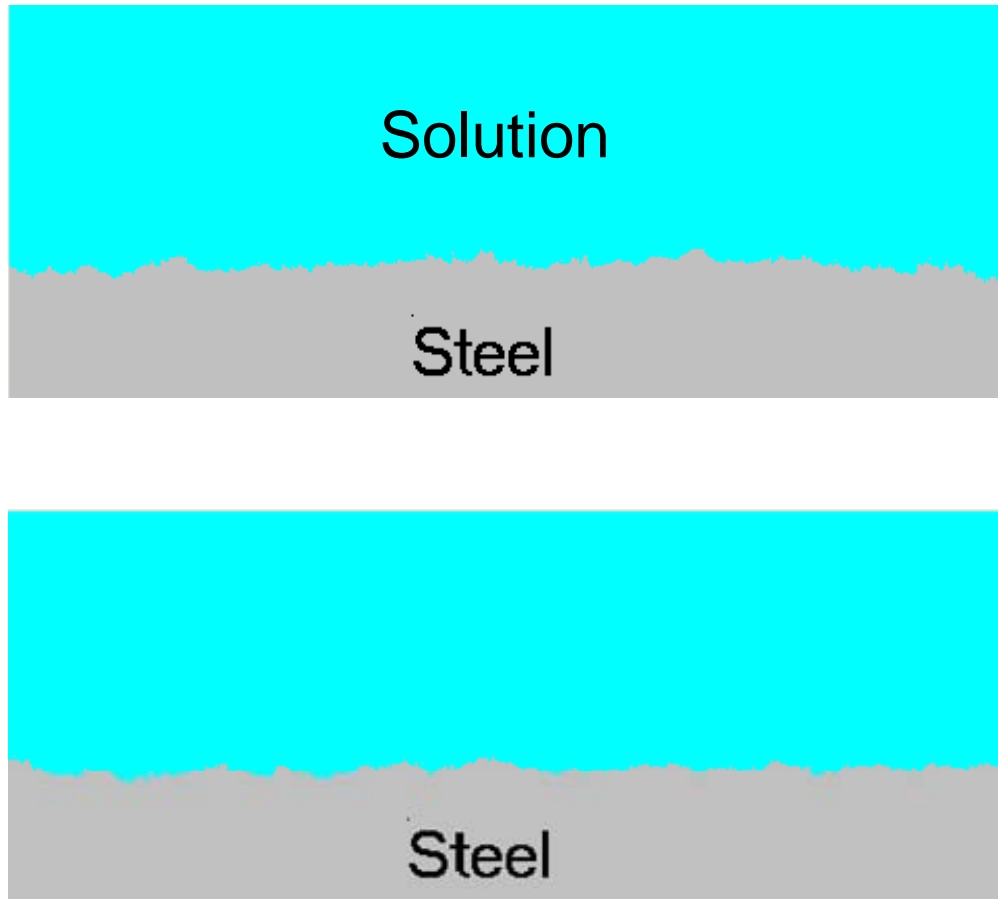


Figure 2.2. Two samples of simulated metal surface morphology following rapid uniform corrosion without any film precipitation. Original Pots's algorithm [1996] was used.

When  $ST$  is set somewhere between value of 0 and 1, the algorithm predicts either an unprotective film with a moderately high corrosion rate for  $ST=0.22$  (see Figure 2.4), or a partially protective film leading to a localized corrosion attack for  $ST=0.37$  (see Figure 2.5). It should be noted that the prediction is stochastic, i.e., even given the same  $ST$  value, the algorithm leads to somewhat different surface morphologies every time the simulation is repeated. Nevertheless, the overall nature of the attack remains the same as illustrated in Figure 2.2-Figure 2.5, where each simulation was repeated twice. This

property matches with the deterministic features in the stochastic pitting process reported by Hoerle [1998]. This implied that the stochastic model can predict localized attack repeatedly as long as the conditions are the same.

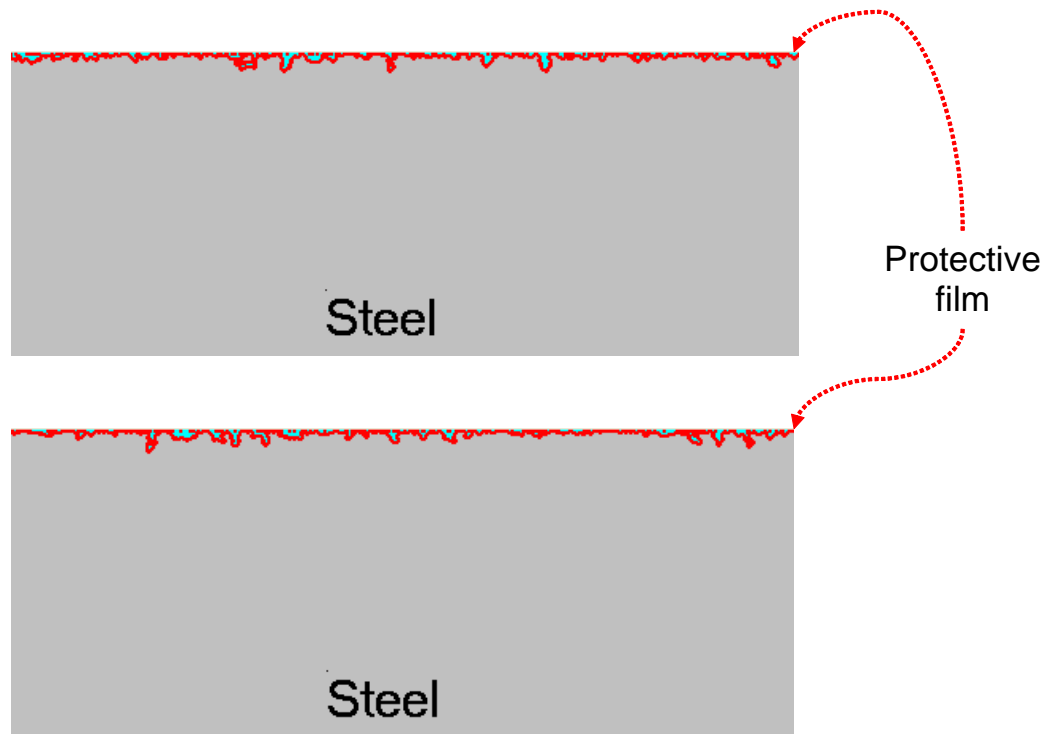


Figure 2.3. Two samples of the simulated metal surface morphology following rapid precipitation, which leads to a protective film and very little corrosion. Original Pots's [1996] algorithm was used.

It is remarkable that one can obtain all these various forms of corrosion attack by varying a single parameter, the scaling tendency. Also interesting is the fact that the algorithm captures the experimental behavior reported by Nyborg [1998] and Sun and Nestic [2003] related to localized corrosion occurring in the “grey zone” when partially

protective films are formed. In order to understand how this happens in the model, it is necessary now to turn attention briefly to the inner workings of this algorithm.

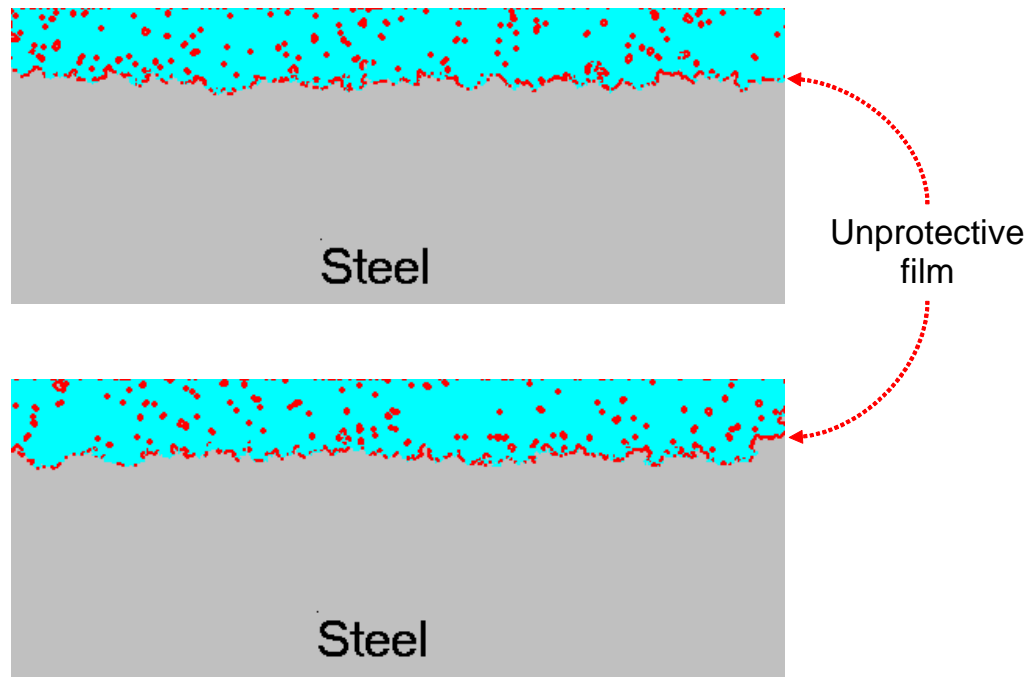


Figure 2.4. Two samples of simulated metal surface morphology following slow precipitation leading to an unprotective film and a moderate corrosion rate. Original Pots's[1996] algorithm was used.

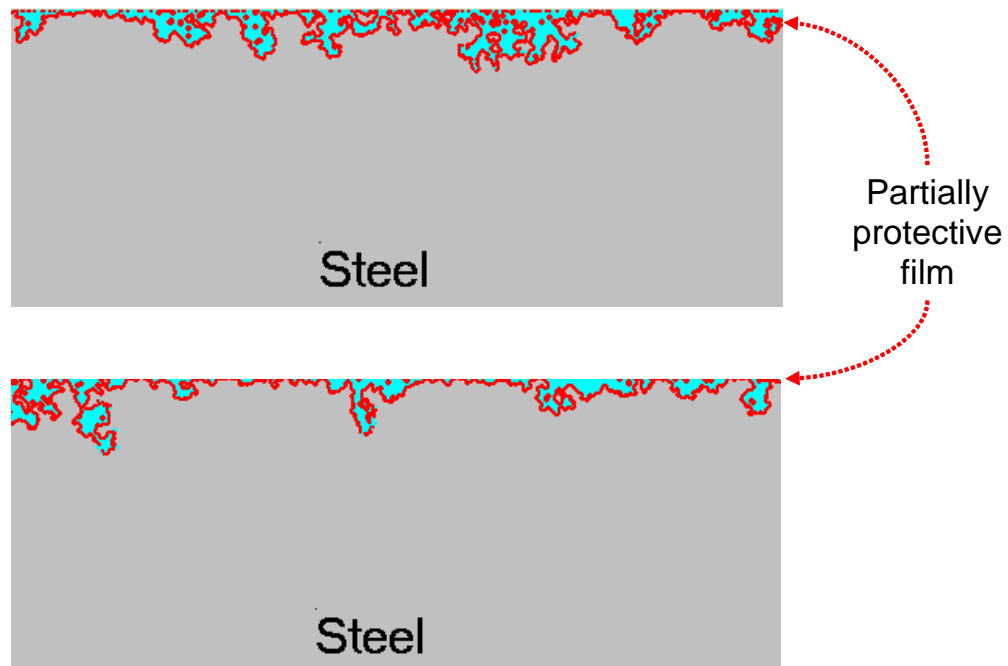


Figure 2.5. Two samples of simulated metal surface morphology following moderate precipitation leading to a partially protective film and localized corrosion. Original Potts's [1996] algorithm was used.

The core of the algorithm is remarkably simple. The steel is graphically represented by a gray  $200 \times 500$  pixels rectangular field on the computer screen. Each pixel represents, in a loose sense, a grain of metal. Since a two-dimensional (2-D) situation is dealt with here, each grain has four sides that may or may not be exposed to corrosion (top, bottom, left and right). It is assumed that initially the corrosive fluid is present only on the topside of the steel. Once the corrosion simulation is started, the algorithm randomly selects a grain on the metal surface. The selected grain is corroded

by decreasing its associated corrosion index ( $CI$ ) by an amount, which is linearly proportional to the number of sides,  $\Theta$ , the grain has exposed to the solution. The rule is:

$$CI_{new} = CI_{old} - 4 \Theta \quad (2-13)$$

According to this rule, the grain which has three sides exposed corrodes (its  $CI$  has been reduced) three time faster than the grain with only one side exposed. Initially, all the grains on the top layer have only one side exposed ( $\Theta=1$ ) and all the other internal grains have no exposed sides ( $\Theta=0$ ). This changes as the simulation progresses and the grains get corroded away. If it happens that all the grains around a particular grain corrode away, that grain with  $\Theta=4$  will become detached and will be removed from the remaining simulation process. Every grain starts out with the same, arbitrarily chosen, corrosion index,  $CI=10$ , and is corroded away when  $CI$  decreases to or below zero. When this happens, the corresponding steel pixel is removed from the simulation. Correspondingly, it changes its color from gray to blue on the computer screen.

During the simulation, precipitation of a film happens along with corrosion in alternating steps. The algorithm performs the precipitation step by randomly selecting a grain where precipitation will happen. Precipitation is simulated by increasing a film index,  $FI$ , for that particular grain. Every grain starts out without any film,  $FI=0$ . If it is hit by precipitation, its film index is increased until  $FI \geq 10$  at which point that this particular grain has a very dense film and is fully protected from corrosion. On the screen, this is demonstrated by a pixel turning red above the protected pixel. Every time the precipitation process randomly “hits” a grain. Then its film index increases by an amount

which is proportional to the number of sides,  $\Theta$ , under the condition that particular grain has exposed to the solution and the scaling tendency,  $ST$ . The rule is:

$$FI_{new} = FI_{old} + 8 \Theta ST \quad (2-14)$$

Obviously when there is no precipitation ( $ST=0$ ), the film index  $FI$  will not change during the simulation. Vice versa, when the precipitation rate is high ( $ST \approx 1$ ), the film index for any particular grain will rapidly reach (in one or two hits) the maximum value of 10, at which point the film is considered to be fully protective.

The simple algorithm described above works remarkably well and produces a wide range of corrosion surface morphologies as already illustrated in Figure 2.-Figure 2.. Even if there is not much explicit physico-chemical content built into the algorithm (other than  $ST$ ), the appearance of the 2-D corroded surface, including the one with localized attack, is rather similar to what is seen in Scanning Electron Microscope (SEM) images of corroded steel samples. This leads us to a conclusion that in order to get localized attack, it is sufficient to have a partially protective film and stochastic corrosion and precipitation processes. On a microscopic level, both the corrosion and the precipitation processes are stochastic in nature due to a constant interchange of cathodes and anodes, inhomogeneous steel surface metallurgy, stochastic nature of the diffusion process, to name just a few arguments. Therefore, it can be concluded that the only condition that is needed to get localized attack is partially protective film, which is the same conclusion that Sun and Nescic [2003] reached by analyzing long-term  $CO_2$  corrosion experiments in wet gas flow. It can be argued that this is a “minimum requirement” for localized

corrosion, notwithstanding the fact that other factors such as hydrodynamics, steel composition, inclusions, etc. might complicate the situation further.

Pots's model works remarkably well to provide all the various forms of corrosion attack by varying a single parameter, the scaling tendency. Since scaling tendency is related to nearly all the primitive parameters that affect localized corrosion, this thesis will use Pots's model as a starting point to build a more advanced localized corrosion model.

## CHAPTER 3

## MODEL DEVELOPMENT

Pots's original algorithm requires only one input: the scaling tendency  $ST$ . This apparent strength is its weakness as well, since knowing  $ST$  is not straightforward.  $ST$  depends on the precipitation rate as well as the corrosion rate as shown by equation (2-12). Neither of the two is easy to be predicted as they depend on many factors including water chemistry, steel composition, surface electrochemistry, transport of species in the solution, etc. Therefore, given that one knows the primitive input parameters such as temperature, pH, velocity, etc., a model is needed to predict the corrosion and precipitation rates, before  $ST$  can be found.

The second weakness of the original algorithm lies in the arbitrariness of the constants used in the rules expressed in the former chapter. The constants in equations (2-13) and (2-14) have been adjusted relative to each other to give plausible answers in terms of morphology of the corrosion attack. However, the answer is qualitative and one cannot deduce the magnitude of the attack, be it uniform or local.

All of the above weaknesses can be overcome and the detailed method will be explained in the following paragraphs. The rules of the original algorithm were also scrutinized and modified to make the simulation perform more reasonably.

Before any modification was carried out, the number of repetitions of the two processes (corrosion and precipitation) for each simulation has been increased 20 times. The maximum depth vs. time curve has been substituted by the maximum penetration

rate vs. time curve because the latter makes more practical sense. Uniform corrosion rate vs. time curve has been calculated and drawn on the same graph.

### 3.1 Modification of the Corrosion Rule

In the original algorithm, the rate of corrosion of any particular grain on the steel surface is proportional to its exposed surface area. In terms of the rules defined above, the decrease of the corrosion index  $CI$  is only proportional to the number of sides -  $\Theta$ , which that particular grain has exposed to the solution (see equation 2-13). However, the corrosion rate of any particular grain should also be related to the presence of a protective film. The algorithm described above takes this into account only in a binary sense, i.e., when the film index,  $FI$ , increases to or above 10, the grain is considered fully protected and cannot be corroded further. What the original algorithm does not take into account is the effect of partially protective film. It is known that surface films range in protectiveness from unprotective to mildly and to very protective depending on their density/porosity. This can easily be accommodated by the rules above as the film index,  $FI$ , which varies from 0 to 10, can be seen as an indicator of film protectiveness. We can assume that the higher the  $FI$  is for a particular grain, the slower it will corrode. Therefore, equation (2-13) can be modified as follows:

$$CI_{new} = CI_{old} - 4 \Theta \left(1 - \frac{FI}{10}\right) \quad FI < 10 \quad (3-1)$$

$$CI_{new} = CI_{old} \quad FI \geq 10 \quad (3-2)$$

When there is no film, i.e., for the grain  $FI=0$ , the equation works in the same way as equation (2-13). However, the change in the grain  $CI$ , i.e., its corrosion rate, slows down as the grain  $FI$  increases due to buildup of a protective film. Eventually, when the film becomes fully protective (the grain  $FI=10$ ), corrosion is hindered and equation (3-1) predicts that the grain  $CI$  stops decreasing. In other words, the modification makes the new algorithm work like the original one at the extremes (no-film and fully protective film situations). What is more important, it adds the intermediate effect of partially protective films.

### **3.2 Modification of Precipitation Rule**

To initiate precipitation, the solution must be supersaturated. The precipitation takes place in two stages: nucleation and growth of these nuclei to macroscopic scale [Calarch 2001]. It is not easy to detect formation of sub-micronic nuclei and generally both nucleation and growth occur simultaneously in solution. It is well known that the addition of small “seed” particles to a supersaturated solution can greatly increase the rate at which crystals nucleate. The classical theory of nucleation provides a natural explanation as to why a seed crystal facilitates crystal nucleation: in order to grow, crystallites of the stable phase need to exceed a critical size. Crystallites that are smaller than this “critical nucleus” dissolve again while larger crystallites can grow to a macroscopic size. In the absence of a seed, a rare, spontaneous fluctuation is needed to form a crystal nucleus that exceeds the critical size [Cacciuto 2004].

Nucleation theory is based upon thermodynamic models which link nucleation rate to supersaturation [Calarch 2001]. According to Johnson [Johnson 1991], scale

nucleation may be related to precipitation rate. At a high precipitation rate, iron carbonate may rapidly nucleate and grow to form a thin tight surface film. At a low precipitate rate, precipitation may proceed so slowly (due to loss of nucleation center) that the crystals either are swept away or grow in irregular islands on the surface.

Nucleation process, which has not been considered in Pots' original algorithm, is implemented in this thesis's model by performing the following precipitation rules:

$$FI_{new} = FI_{old} + 4\Theta ST \quad t > t_{crit} \quad (3-3)$$

$$FI_{new} = FI_{old} + 4\Theta ST \frac{t^A}{t_{crit}^A} \quad 0 < t < t_{crit} \quad (3-4)$$

where  $A$  is a constant greater than one. The value of  $A$  and its physical meaning are demonstrated below. Here it is assumed that there exists a time period that both nucleation and crystal growth account for the increase of film index. The reason is that it takes time for iron carbonate to aggregate, to form crystals that exceed a critical size, and then to precipitate. Beyond that time period, this barrier disappears when a large amount of crystallites form. Then only crystal growth, which can be represented by precipitation rate, could influence the increase of film index. This period of time is defined as the time interval from the beginning to a critical time, which is controlled by super saturation [Calarch 2001]. From equation (2-10), it is known that super saturation is related to  $R_{PR}$ , and  $R_{PR}$  is proportional to  $ST$ . So  $t_{crit}$  is related to  $ST$ . Higher  $ST$  results in smaller  $t_{crit}$ . So  $t_{crit}$  is reversely proportional to  $ST$ . During the period of time between  $t=0$  and  $t=t_{crit}$ , it is assumed that the precipitation rate is increased from 0 (when  $t=0$ ) to its full developed rate  $4\Theta ST$  (when  $t=t_{crit}$ ) with a quadratic function with respect to time. That means  $A$

$=2$ , which is determined by comparing to experimental data. The chosen value of  $A$  demonstrates that the precipitation is harder at the beginning of process when there are no or little nuclei in the system. With the increase of the amount of nuclei, precipitation becomes easier.

Note that the constant that determines how fast the film will precipitate has been decreased from 8 in equation (2-14) to 4 in equation (3-3) and (3-4) to balance the decrease of corrosion rate which resulted due to the modified rules.

The effect of the modified rules on localized attack is illustrated in Figure 3.1. A larger variety of surface morphologies are now obtained over a broader range of  $ST$ . Pits are narrow toward the bottom as well as “mushroom” style pits appear at various  $ST$ . In certain cases, pits propagate much deeper and even fail to heal.

Various steel surface morphologies obtained in the simulations are compared with selected SEM images taken from a  $\text{CO}_2$  corrosion study in multiphase flow by Nescic and Lunde [1994] (see Figure 3.2.). It clearly confirms that the algorithm proposed above is capable of predicting qualitatively a wide range of localized attack morphologies seen in practice.

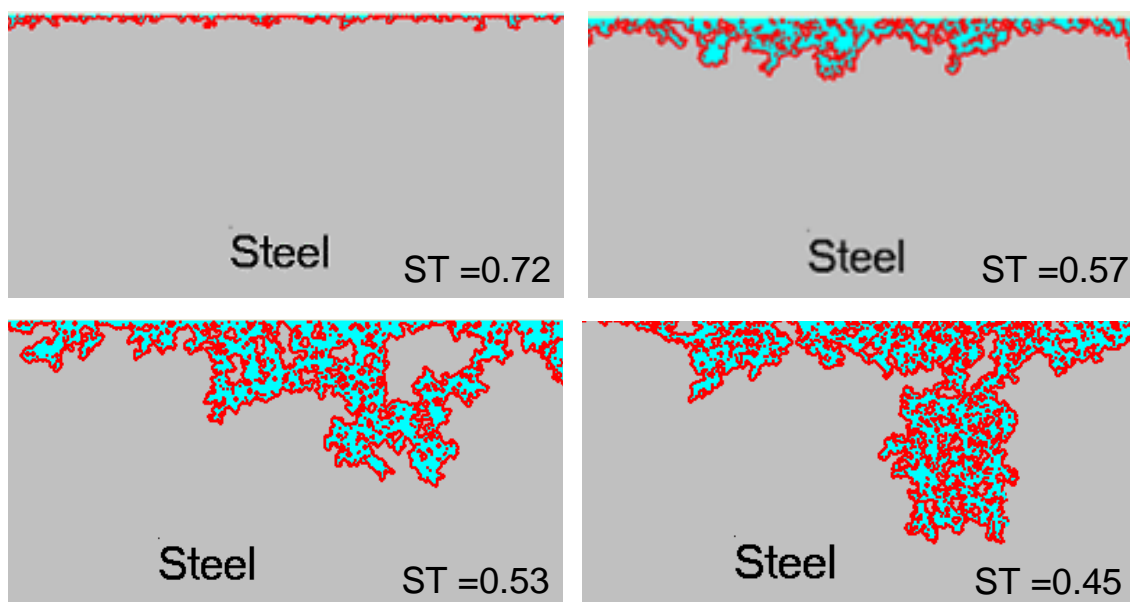


Figure 3.1. Surface morphology prediction taken from the study of 2-D localized corrosion model by Nescic, Xiao, and Pots [2004]

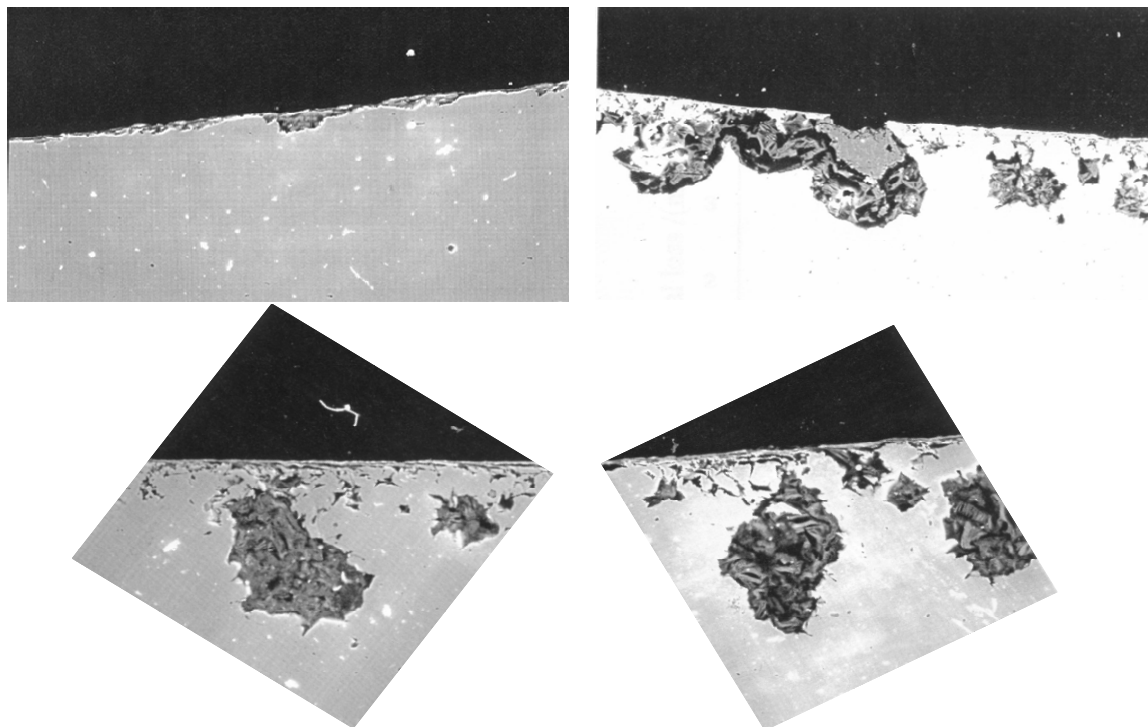


Figure 3.2. SEM images of the corroded steel surfaces taken from the study of  $\text{CO}_2$  corrosion in multiphase flow taken from the study by Nescic and Lunde [1994].

### 3.3 Link to OU 1-D Mechanistic Model

As mentioned at the beginning of this chapter, there are two obvious weaknesses in Pots's original algorithm. One is that the model only depends on  $ST$  and another is that its value is not easier to be obtained. Both weaknesses can be eliminated by linking the algorithm with a corrosion/precipitation model that can predict the scaling tendency  $ST$  and uniform corrosion rate. Hence, the morphology and the magnitude of the attack can be predicted. For this purpose, the mechanistic one-dimensional (1-D)  $CO_2$  corrosion model of Netic [2003] has been used in this thesis.

For the purposes of connecting it with the 2-D algorithm described above, it is required to compute the scaling tendency at the steel surface where the films form. Therefore one needs information about the solution chemistry at the steel surface, which can be very different from the one in the bulk, particularly if some sort of surface film is already in place. Further, the scaling tendency changes with time as the corrosion and precipitation rate change. Very few corrosion/precipitation models can satisfy this requirement.

The recent 1-D mechanistic model of Netic [Nordsveen 2003, Netic and Lee 2003, Netic 2003] is a perfect candidate for linkage with the 2-D algorithm described above as it computes concentration profiles of all species involved in the corrosion/precipitation reactions. The model covers most of the important processes present in uniform  $CO_2$  corrosion of carbon steel:

- Electrochemical reactions at the steel surface,

- Chemical reactions including precipitation and
- Transport of species between the steel surface and the bulk solution including transport through the porous corrosion film.

The physical, mathematical and numerical aspects of the proposed model are explained in detail in the original papers; however a very brief outline is given below to facilitate the understanding of the text to follow. Since it is a model of uniform corrosion, a one-dimensional computational domain is used, stretching from the steel surface through the pores of a surface film and the mass transfer boundary layer, ending in the turbulent bulk of the solution. Detail description of this model can be found in Nescic *et al.* [Nescic and Lee 2003, Nescic and Nordsveen 2003, Nescic 1996] paper.

The concentration of each species is governed by a species conservation (mass balance) equation. A universal form of the equation which describes transport for species  $j$  in the presence of chemical reactions, which is valid both for the liquid boundary layer and the porous film, is:

$$\underbrace{\frac{\partial(\varepsilon c_j)}{\partial t}}_{\text{accumulation}} = \underbrace{\frac{\partial}{\partial x} \left( \varepsilon^{1.5} D_j^{eff} \frac{\partial c_j}{\partial x} \right)}_{\text{net flux}} + \underbrace{\varepsilon R_j}_{\substack{\text{source or sink} \\ \text{due to chemical reactions}}} \quad (3-5)$$

where  $c_j$  is the concentration of species  $j$  in  $kmol m^{-3}$ ,  $\varepsilon$  is the porosity of the film,  $D_j^{eff}$  is the effective diffusion coefficient of species  $j$  (which includes both the molecular and the turbulent component) in  $m^2 s^{-1}$ ,  $R_j$  is the source or sink of species  $j$  due to all the chemical reactions in which the particular species is involved in  $kmol m^{-3} s^{-1}$ ,  $t$  is time and  $x$  is the

spatial coordinate in  $m$ . It should be noted that in the transport equation above electromigration has been neglected as its contribution to the overall flux of species is small. Turbulent convection has been replaced by *turbulent diffusion* as the former is difficult to determine explicitly in turbulent flow.

One equation of the form (3-5) is written for each species. They all are solved simultaneously in space and time. The boundary conditions for this set of partial differential equations are: in the bulk - equilibrium concentrations of species (which is also used as the initial condition), and at the steel surface - a flux of species is determined from the rate of the electrochemical reactions (zero flux for non-electroactive species). Once the set of equations is solved in any given time step, the uniform corrosion rate,  $CR$ , can be simply calculated as the flux of  $Fe^{2+}$  ions at the metal surface.

Solid iron carbonate ( $FeCO_3$ ), which is treated as one of the species, will precipitate when the iron carbonate saturation exceeded according to (2-5).

From the two different expressions describing the kinetics of iron carbonate precipitation proposed by Johnson [1991] and Van Hunnik [1996], the latter (equation 2-10) is used because it is believed to give more realistic results especially at higher super saturation.

Once the rate of precipitation,  $R_{FeCO_3(s)}$ , and the uniform corrosion rate,  $CR$ , are calculated as a function of the input parameters such as temperature, pH, partial pressure of  $CO_2$ , velocity, etc., the scaling tendency  $ST$  can be computed according to equation (2-12) and used as an input into the 2-D model.

Table 1 lists the test conditions used to calibrate the 1-D mechanistic model and 2-D localized corrosion model. Since different *ST* give different morphologies of surface, table 1 lists conditions that will give a variety of *ST*. Some film forming conditions are also listed to calibrate the precipitation rate and hence to obtain the maximum penetration rate.

Table 1. Test Matrix

Parameters	Conditions
CO <sub>2</sub> partial pressure (bar)	2, 1, 0.54
Solution	1% NaCl, distillation water
pH	5.8, 6.0, 6.3, 6.5, 6.6
single-phase flow (m/s)	1, 0.2
Temperature (°C)	50, 55, 65, 80
Test time (hrs)	50
Iron concentration (ppm)	5, 25, 50, 100

An illustration of the integrated 2-D model at work is shown in Figure 3.3. Under those conditions one gets a very protective film at pH6.6, only a partially protective film and some initial localized attack (which heals) at pH6.3, poorly protective film and progressive localized attack at pH6.26 and unprotective films and uniform attack at pH6.2 and lower.

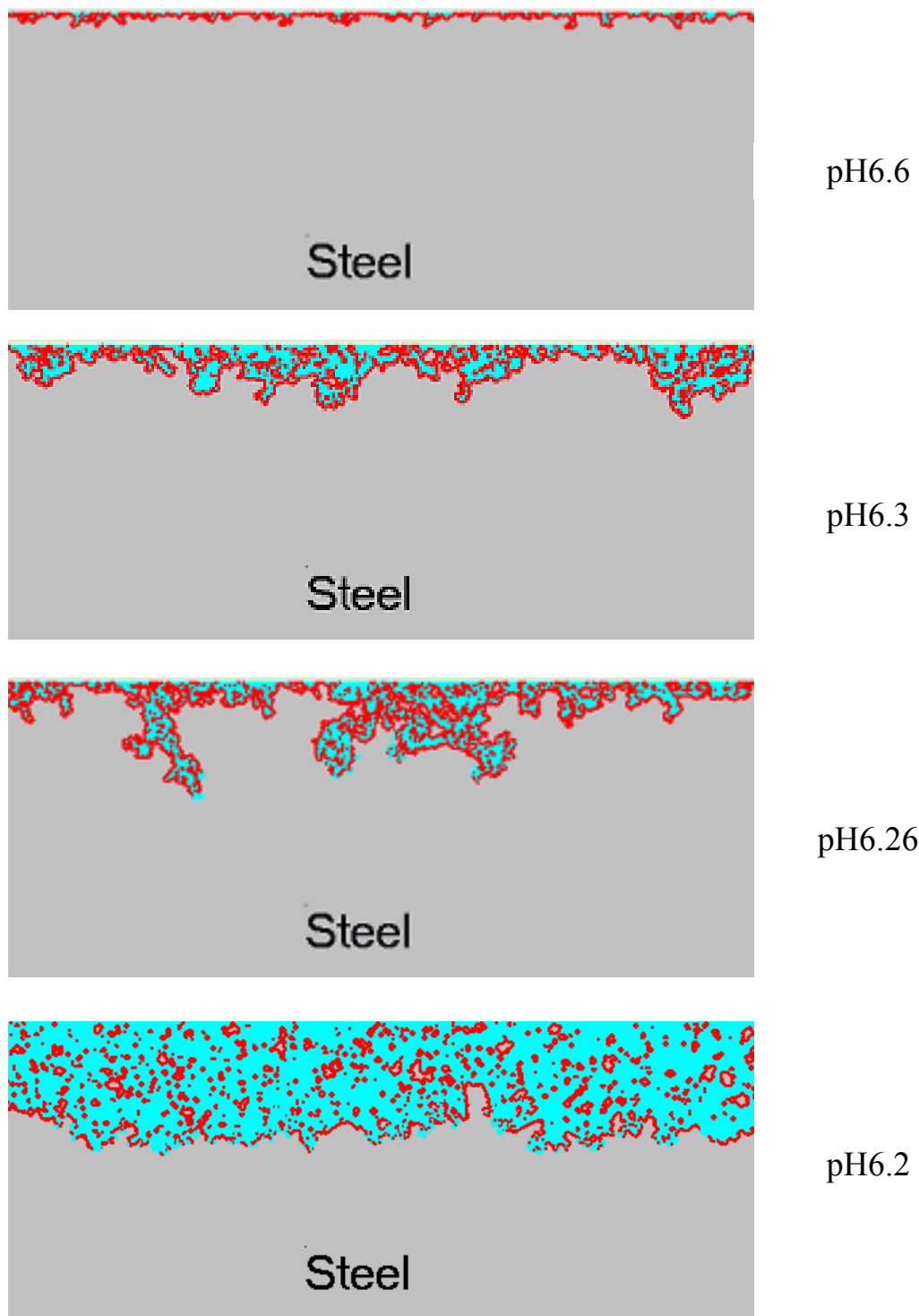


Figure 3.3. Predictions for the case of a 1%NaCl solution, at  $T = 80^{\circ}\text{C}$ ,  $P_{\text{CO}_2} = 0.52\text{bar}$ ,  $P_{\text{total}} = 1\text{bar}$ ,  $C_{\text{Fe}^{2+}} = 100\text{ppm.}$ ,  $v=1\text{ m/s}$ .

### 3.4 Film Growth Algorithm

Film precipitation is one of the two crucial processes in this simulation, and the rules it performs have been fully described in equations (3-3) and (3-4). But the growth of the film has not been considered in the previous work, and neither has its effect on corrosion. As we know, in reality, as long as the solution is supersaturated, iron carbonate will continuously precipitate and layers upon layers of films form. Thus, a film growth algorithm needs to be implemented to make the whole simulation perform more realistically.

The film grows according to the precipitation rate. As mentioned above, when a grain is hit by a random film process, its *FI* will be increased based on equation (3-3) or (3-4). If the film index is above 10, film forms. In the previous work, the simulation did not perform differently when the film index was greater than 10, because film growth was not built in. However, film index is a good indicator to be used for predicting the thickness of the film.

The film can protect not only the steel grain it covers on top but also to some extent its neighbors. As each grain has four neighbors, there are four possible exposed sides. A film that precipitates on any of the four neighbors hinders the corrosion of that specific grain from that side, and the possibility for that specific grain to corrode decreases as the number of exposed sides decrease. The influence of this effect is more obvious when the film grows quickly.

The film is more stable when the  $ST$  is high because higher  $ST$  usually results in protective film. When the precipitation rate is high compared to uniform corrosion rate, the film is denser and the distance between the film and bare metal is shorter, which means the film is more resistant to being swept away by the flow [Johnson 1991]. On the contrary, when the precipitation rate is low compared to corrosion rate, the formed film is more porous and the distance between the film and bare metal could be quite large and hence, could easily be removed by the flow. So, the ability for the next layer of film to grow varies with surface scaling tendency. Even at the same surface scaling tendency, the film grows easier when it is close to metal surface due to less turbulence reaching the surface through the boundary layer. This is modeled by the following equation i.e. when a

$$FI > (L + 1) * 10 * A^{L*(1-ST)} \quad (3-6)$$

then a new film layer forms. Here  $L$  represents the number of layers of film for a specific steel grain.  $A$  is a constant greater than 1. This formula clearly shows that the higher the scaling tendency is, the easier it is for the next layer of film to form; the smaller the  $L$  is, the easier it is for the next layer of film to form. The values of  $A$  and  $L$  need to be calibrated with experimental data.

The algorithm of iron carbonate film growth was implemented in an easy way at first. It was considered the film deposited directly on top of the previous film. Figure 3.4 shows typical film morphology obtained in simulation studies. From this figure, a clear solution layer, a porous film layer, a dense film layer, and the detached layer between film and metal can be easily observed from top to bottom. Comparison with the various

film morphologies on the selected SEM image (see Figure 3.5) taken from a CO<sub>2</sub> corrosion precipitation study by Lee [2003], confirms the existence of all the above layers.

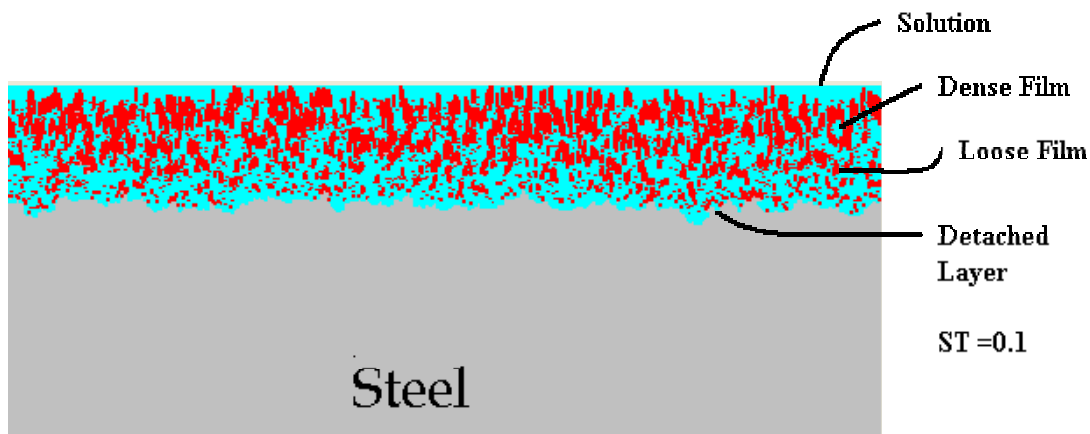


Figure 3.4 Film morphology taken from the proposed 2-D Model.

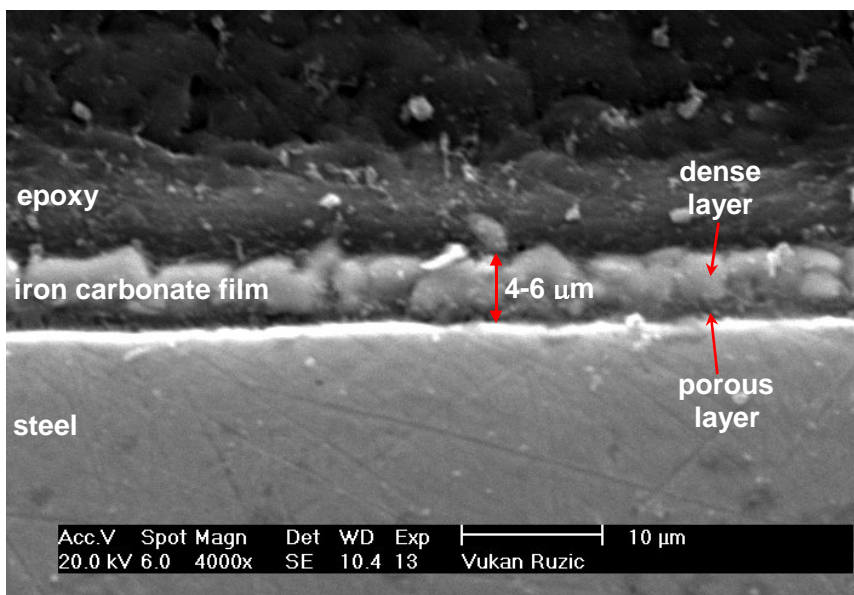


Figure 3.5 SEM image of a cross section of a steel specimen including an iron carbonate film. Exposed for 10 hours at  $T=80^{\circ}\text{C}$ ,  $\text{pH } 6.6$ ,  $P_{\text{CO}_2} = 0.54 \text{ bar}$ ,  $c_{\text{Fe}^{2+}} = 250 \text{ ppm}$ ,  $v=1 \text{ m/s}$ .

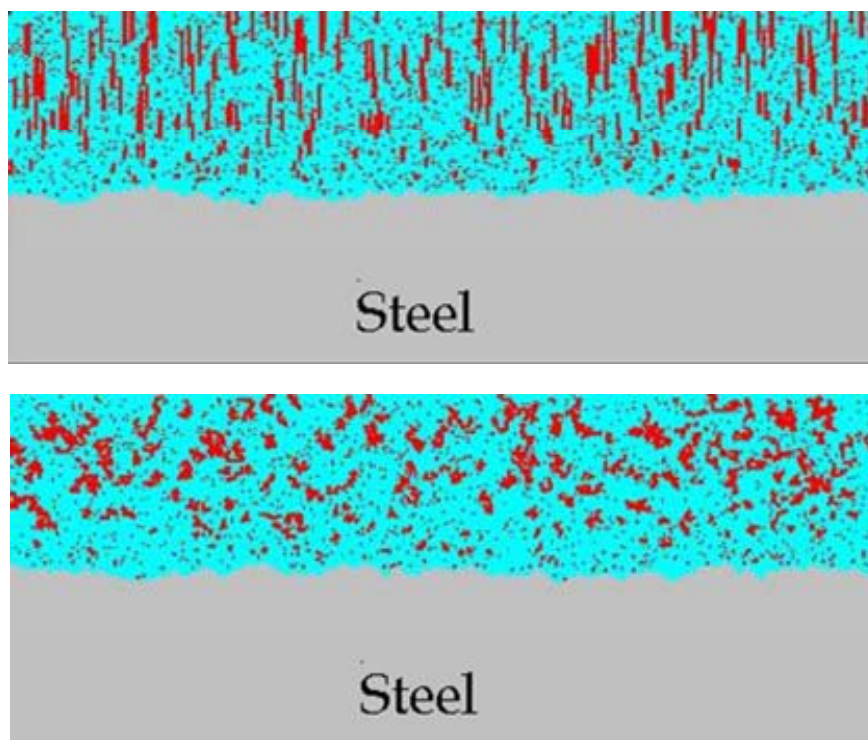


Figure 3.6 Comparison of the film morphology before (top) and after (bottom) using a random film formation algorithm at pH 6.6, 80°C, 5ppm  $\text{Fe}^{2+}$  and 0.52bar  $\text{pCO}_2$ .

The computer screen displays only part of the film, which grows in the domain of the original piece of metal. Actually, the film could grow far beyond the location of the original piece of metal out to the bulk. But in order to create a tidy display, we chose not to show it.

From Figure 3.4, it is seen that the structure of the film does not seem realistic. In reality, the film deposits randomly in any direction instead of only vertically. And the structure of crystallites is more porous with self similarity properties like fractals [Joosten 1992]. Fractals are objects with self-similar structures on different scales. In the present model, a random process has been implemented to allow the next layer of film to choose the direction it deposits. The direction could be left, right and top, and the newly formed

film structure is more porous than the previous one. Figure 3.6 and 3.7 show the comparison of the film structures.

The new film structure expands more horizontally than vertically and this property affects the coverage of the surface around the center of the film deposition. From figure 3.8, we see that the shape of the pit becomes more bowl-like with this modification, while it is sharper in the previous version of the model.

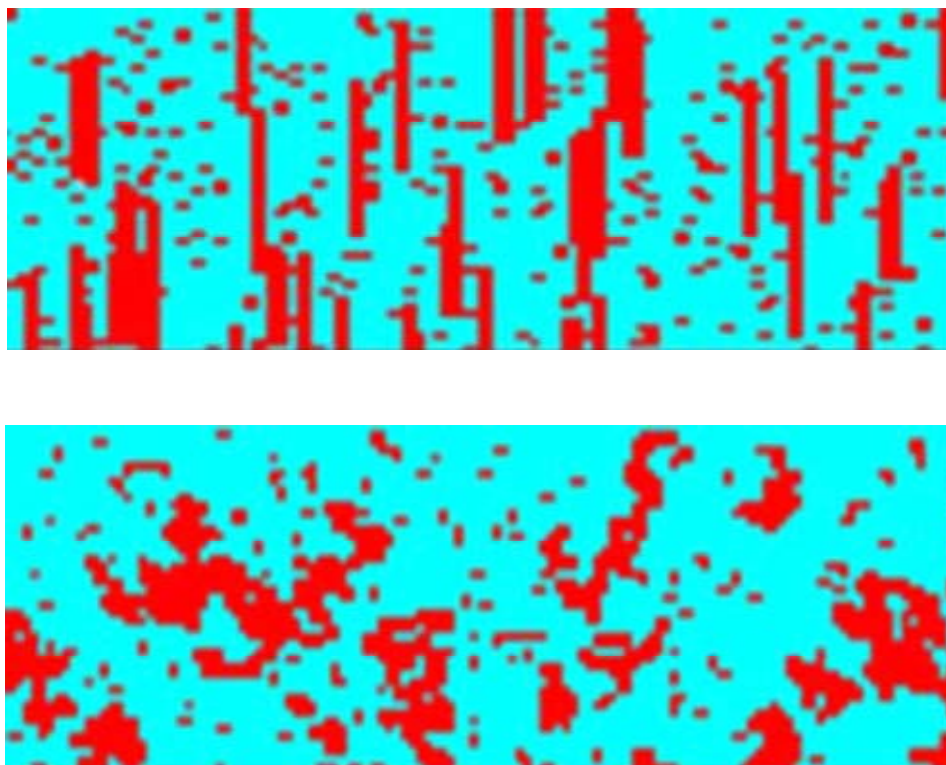


Figure 3.7 Comparison of the film morphology at higher magnification before (top) and after (bottom) using a random film formation algorithm at pH 6.6, 80°C, 5ppm  $\text{Fe}^{2+}$  and 0.52bar  $p_{\text{CO}_2}$ .

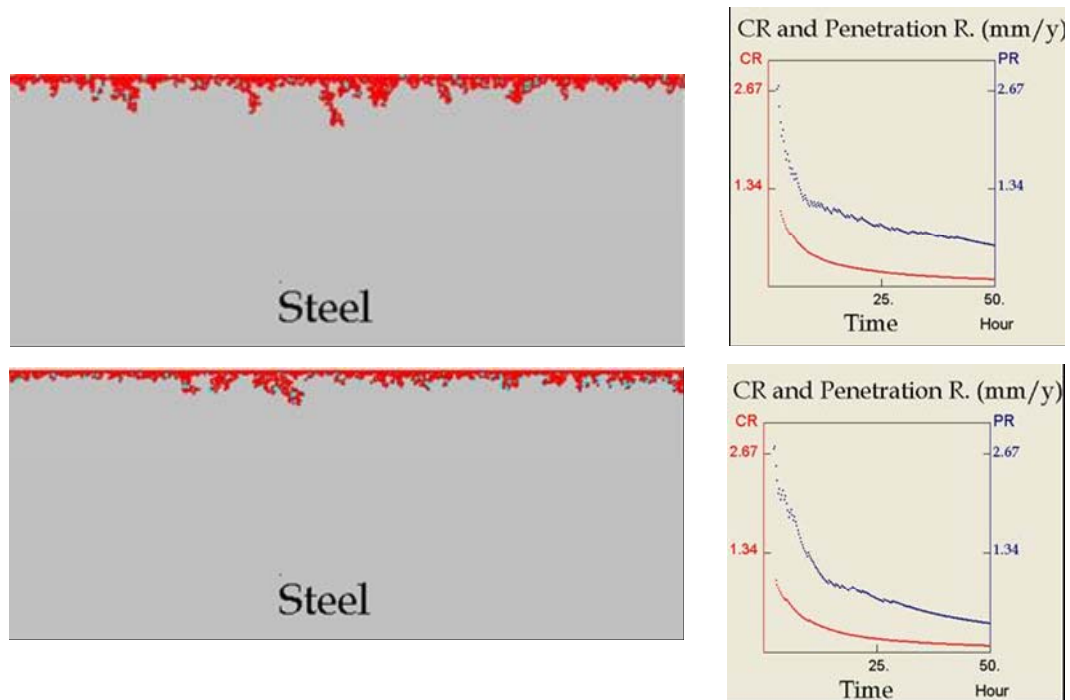


Figure 3.8 Comparison of the film morphology before (top) and after (bottom) using a random film formation algorithm at pH 6.5, 80°C, 50ppm  $\text{Fe}^{2+}$  and 0.52bar  $p_{\text{CO}_2}$ .

### 3.5 Implementation a Path-Searching Algorithm to Remove Isolated Islands

During a uniform corrosion process, the anodic and cathodic anodes switch back and forth so that the metals at different locations corrode with the same rate. When an iron carbonate film forms, the surface condition is not the same any more because of the protective property of the iron carbonate film. Part of the surface base could still be exposed, leaving the other parts protected. As the protected part of the surface becomes passivated and becomes a cathode, the exposed surface as the anode corrodes more quickly due to large surface ratio of cathode to anode ( $S_c/S_a$ ). Subsequently, a rough

surface forms and some metal could be detached from the base due to the corrosion occurring beneath them (undercutting).

This phenomenon has been observed experimentally. According to Jaycock [1998], pitting tends to undercut the surface, forming lacy covers (lace like structure) that help them to maintain a concentrated local chemistry. At the edges of the pit, transport of metal ions into bulk solution is relatively rapid and the local concentration falls below the critical value, causing these areas to repassivate. Deeper into the pit cavity, active dissolution continues such that pit growth undercuts the passivated material and eventually breaks through the surface from beneath. Metal ions diffuse rapidly through the new hole, again causing the local concentration to fall and repassivation to occur.

This phenomenon also has been noticed in the 2-D simulation. One simulation result shown in Figure 3.9 was selected from original Pots' algorithm, because it shows a better vision for those isolated islands than the present 2-D model, since no films layer was shown in his algorithm and hence the solution is rather clean.

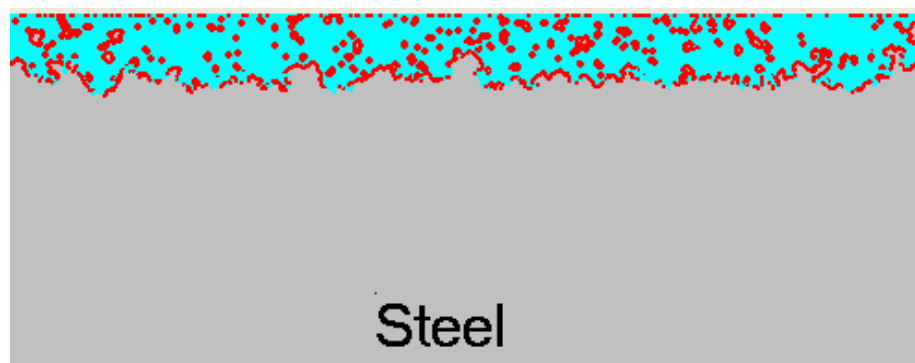


Figure 3.9 Image for isolated islands taken from original Pots' algorithm at  $ST=0.31$

Since the metal is detached from the surface, the weak physical-chemical bond between the metal and the surface base cannot compete with the wall shear stress caused by flow. Therefore, this detached piece of metal should be removed from the simulation domain. This is a mechanical process, rather than an electro-chemical process. A path-searching algorithm is implemented in the model to remove those isolated metal grains. Figure 3.10 to Figure 3.12 show the comparison of the changes caused by implementing this algorithm.

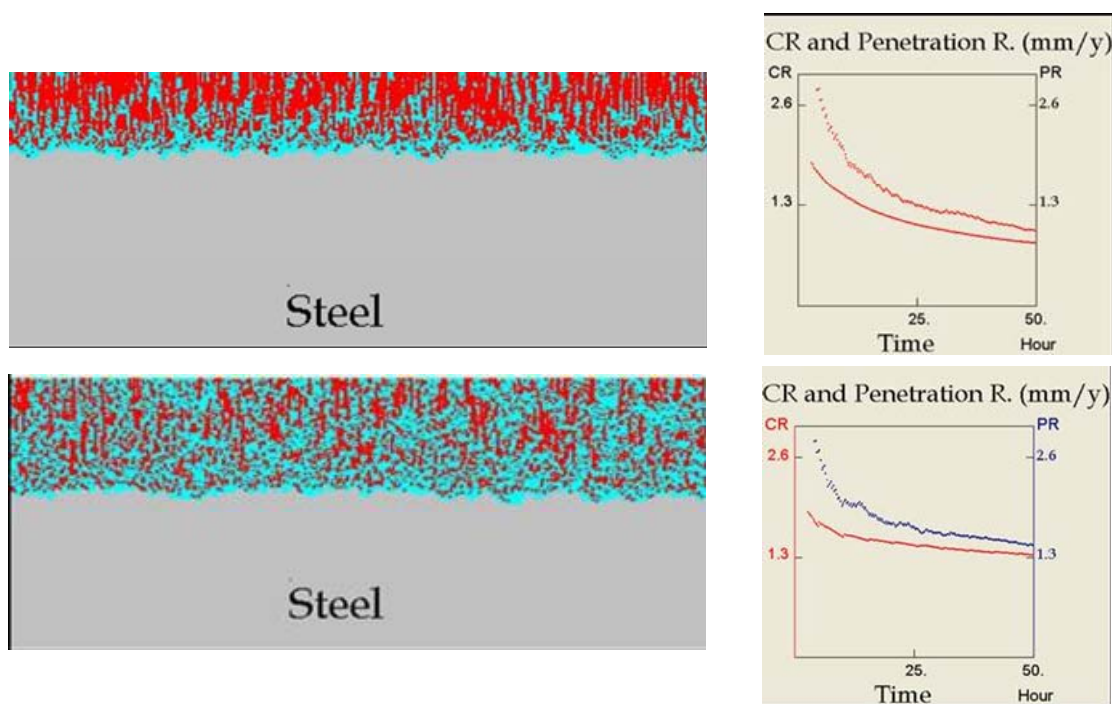


Figure 3.10. Comparison of the surface morphology, uniform corrosion rate and maximum penetration rate before (bottom) and after (top) implementing path-searching algorithm at pH 6.26, 80°C, 50ppm  $\text{Fe}^{2+}$  and 0.52bar  $p_{\text{CO}_2}$ .

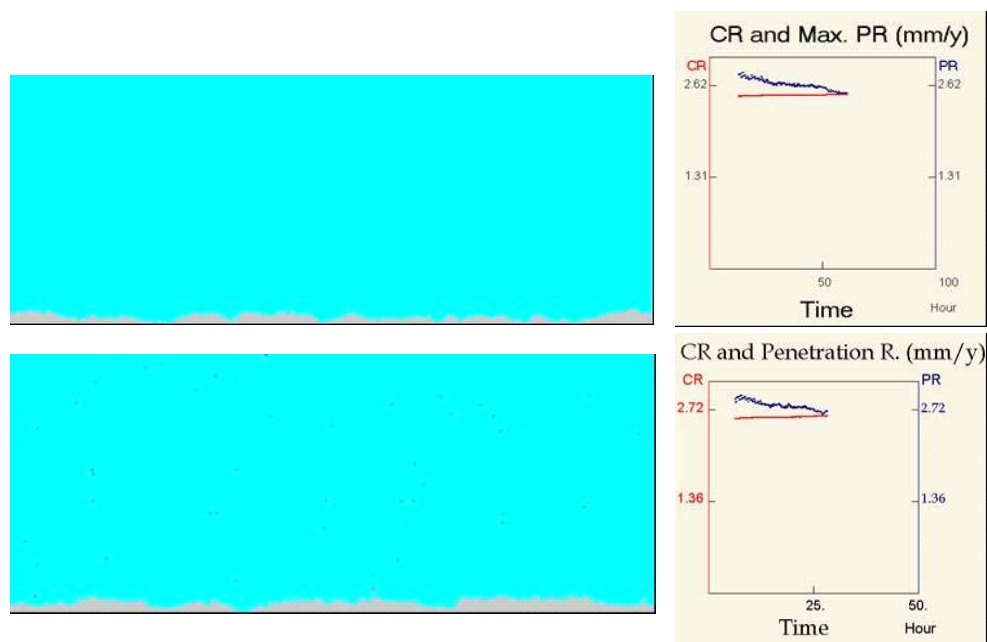


Figure 3.11. Comparison of the surface morphology, uniform corrosion rate and maximum penetration rate before (bottom) and after (top) implementing path-searching algorithm at pH 6.0, 80°C, 50ppm  $\text{Fe}^{2+}$  and 0.52bar  $p_{\text{CO}_2}$ .

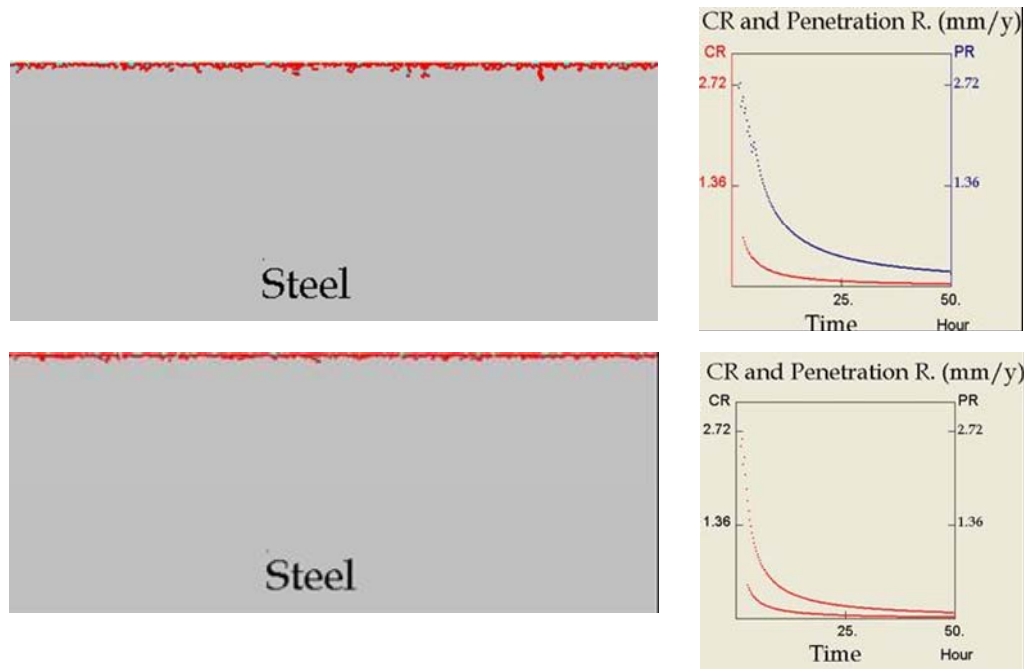


Figure 3.12. Comparison of the surface morphology, uniform corrosion rate and maximum penetration rate before (bottom) and after (top) implementing path-searching algorithm at pH 6.6, 80°C, 50ppm  $\text{Fe}^{2+}$  and 0.52bar  $p_{\text{CO}_2}$ .

After implementing the path-searching algorithm, the predictions of uniform corrosion rate increases for all the conditions due to the remove of isolated islands. Uniform corrosion rates increase a lot under the general localized corrosion condition, where a lot of isolated islands form (see Figure 3.10); while they increase little under localized attack conditions or general uniform conditions (see Figure 3.11 and Figure 3.12). Maximum penetration rates follow the same trend as uniform corrosion rates.

### 3.6 Localized Corrosion Tendency

A pitting factor can be used [Jones 1996] to quantify the seriousness of pitting. It is defined as follows:

$$f = \frac{PR}{CR} \quad (4-7)$$

where,  $f$  = pitting factor;

$PR$  = maximum penetration rate in mm/yr;

$CR$  = uniform corrosion rate in mm/yr.

A pitting factor of unity indicates uniform corrosion. The higher the pitting factor is the higher tendency to occur localized corrosion. A pitting factor of 3 means the maximum penetration rate is 3 times faster than the uniform corrosion rate. Hence, when pitting factor is 3 or above, it indicates that localized corrosion occurs.

## CHAPTER 4

### VERIFICATION

#### 4.1 Comparisons

The present 2-D model has been successfully linked with the 1-D Mechanistic Model and can predict the uniform corrosion rate for different pH, temperature, partial pressure of CO<sub>2</sub>, *etc.* Comparison of the 2-D prediction with 1-D prediction and selected LPR experimental results taken by Chokshi [2004] at the Institute of Corrosion and Multiphase Technologies is shown in Figure 4.1, Figure 4.3, and Figure 4.5. Comparisons of film morphologies between 1-D Mechanistic model and 2-D model are shown in Figure 4.2, Figure 4.4, and Figure 4.6. Figure 4.1 and 4.2 are results under the same condition, same for Figure 4.3 and Figure 4.4, and Figure 4.5 and Figure 4.6.

Since the inputs of the 2-D model are the uniform corrosion rate and surface scaling tendency predicted by 1-D model, it is not surprising that the initial uniform corrosion rate predicted by 2-D simulation agrees with the result from 1-D prediction very well. But the agreement on the morphology of the film and the changing uniform corrosion rate demonstrates that the 2-D stochastic model does perform reasonably well on the basis of 1-D prediction model. A localized corrosion is predicted to occur due to the high pitting factor of 4.4 at pH 6.6, 80°C, 0.52bar p<sub>CO<sub>2</sub></sub>, 50ppm Fe<sup>2+</sup>, and rpm=0.

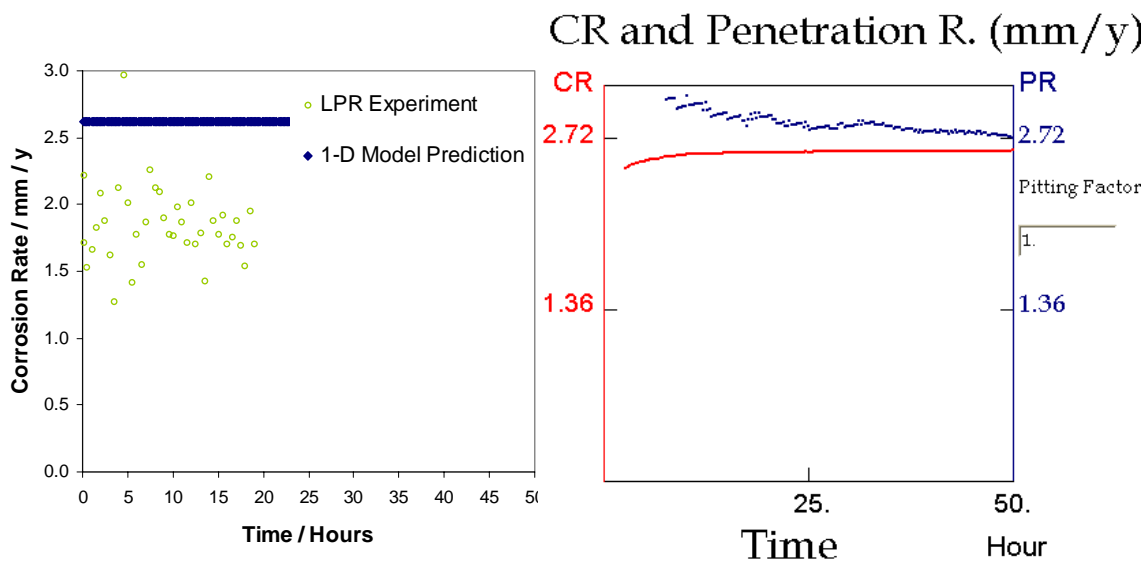


Figure 4.1. Comparison of uniform corrosion rate between LPR experimental result, 1-D prediction, and 2-D prediction at pH 6.0, 80°C, 0.52bar  $p_{CO_2}$ , 50ppm  $Fe^{2+}$ , and rpm=0.

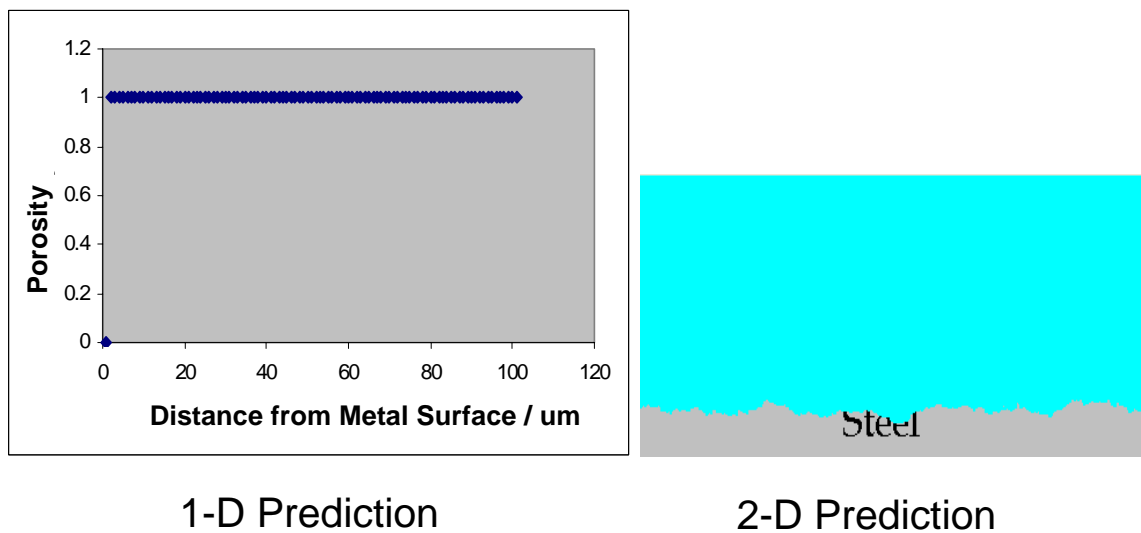


Figure 4.2. Comparison of film morphology between 1-D prediction, and 2-D prediction at pH 6.0, 80°C, 0.52bar  $p_{CO_2}$ , 50ppm  $Fe^{2+}$ , and rpm=0.

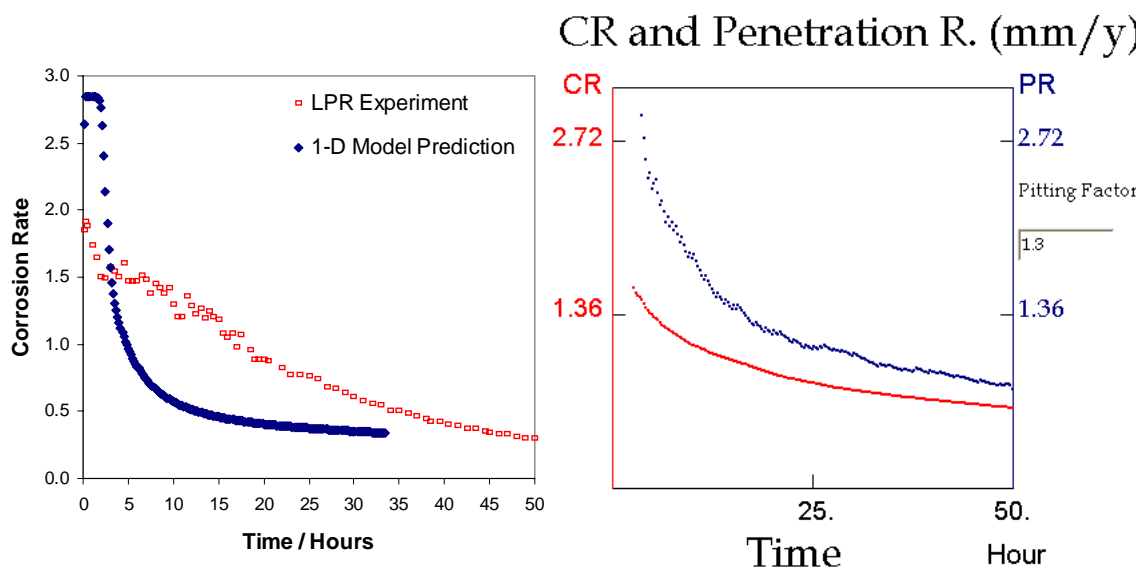


Figure 4.3. Comparison of uniform corrosion rate between LPR experimental result, 1-D prediction, and 2-D prediction at pH 6.3, 80°C, 0.52bar  $p_{CO_2}$ , 50ppm  $Fe^{2+}$ , and rpm=0.

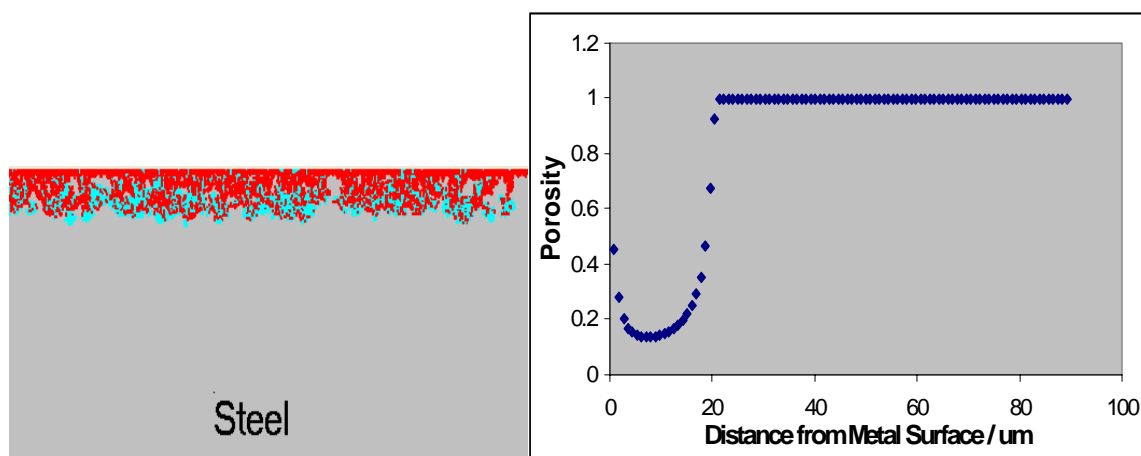


Figure 4.4. Comparison of film morphology between 1-D prediction, and 2-D prediction at pH 6.3, 80°C, 0.52bar  $p_{CO_2}$ , 50ppm  $Fe^{2+}$ , and rpm=0.

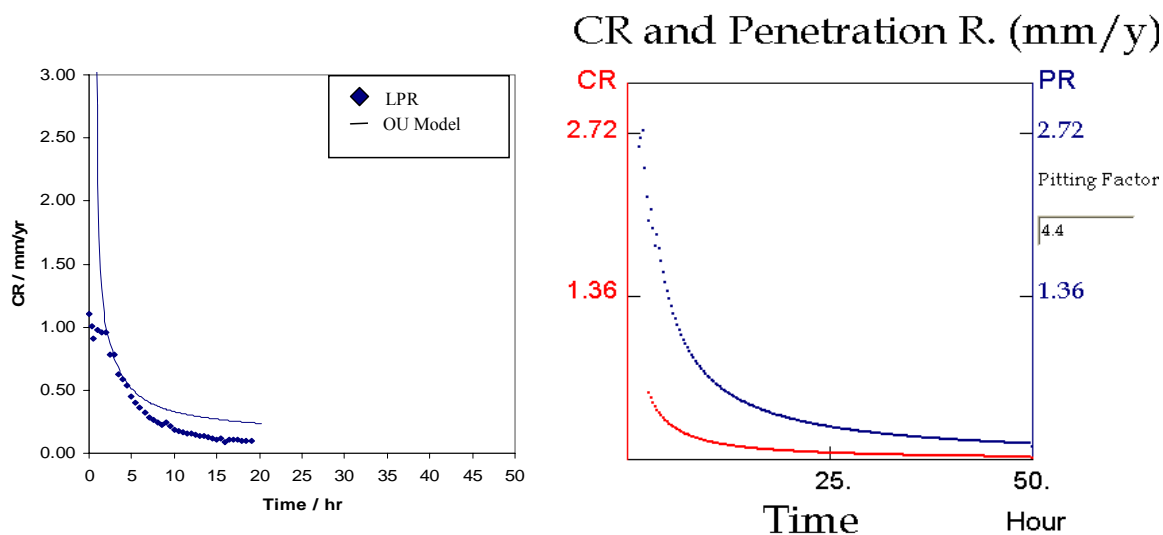


Figure 4.5. Comparison of uniform corrosion rate between LPR experimental result, 1-D prediction, and 2-D prediction at pH 6.6, 80°C, 0.52bar  $p_{CO_2}$ , 50ppm  $Fe^{2+}$ , rpm=0.

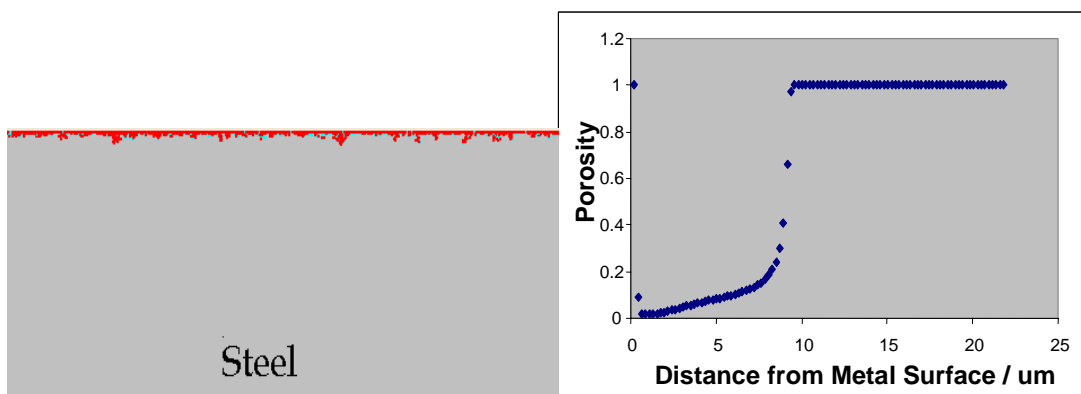


Figure 4.6. Comparison of film morphology between 1-D prediction, and 2-D prediction at pH 6.6, 80°C, 0.52bar  $p_{CO_2}$ , 50ppm  $Fe^{2+}$ , rpm=0.

## 4.2 Parametric study

The surface morphologies and uniform corrosion rate vs. time curve predicted by the 2-D model are shown in Figure 4.7, Figure 4.8, Figure 4.9, Figure 4.10, Figure 4.11, Figure 4.12, and Figure 4.13 by varying ferrous iron concentration for all other conditions

being fixed: 0.54bar  $p_{\text{CO}_2}$ , 80 °C, pH 6.6, 1m/s. In figure 4.7, we see that when there is no  $\text{Fe}^{2+}$  in the solution there is no iron carbonate film formed. The uniform corrosion rate doesn't change with time and uniform attack (2.6 mm/y) is obtained with a unity pitting factor. At  $\text{Fe}^{2+}=5$  ppm there is some precipitation and a porous film forms comprised of large crystals (see Figure 4.8). The uniform corrosion rate decreases slowly and the final uniform corrosion rate reduces by approximately 50%. The pitting factor of 1.1 represents that it is a uniform attack. As the  $\text{Fe}^{2+}$  concentration is increased to 10 ppm and 25 ppm more film precipitates (see Figure 4.9 and 4.10), and the uniform corrosion rate decreases more rapidly to a steady state value of 1.3 and 1.1 mm/y respectively. The films are still porous with smaller grain size, yet not protective and there is no localized attack with pitting factor of 1.1 and 1.3 respectively. Further increase of  $\text{Fe}^{2+}$  concentration to 28 ppm leads to even more film formation however, it takes the conditions into the "grey zone" and localized attack is initiated just as Sun has observed in experiments. The rate of localized attack is approximately 0.7 mm/y while the uniform corrosion proceeds at less than 0.1 mm/y. This leads to a high pitting factor of 5.9. Further increase in  $\text{Fe}^{2+}$  concentration to 30 ppm also results in initial localized attack with a pitting factor of 3.7, however most of the pits heal and both the uniform and localized rates of attack are low. Finally 50 ppm of  $\text{Fe}^{2+}$  results in stable formation of protective films with very little corrosion. The pitting factor of 4.4 is still rather high, and the serious localized corrosion could occur with maximum penetration rate of 0.15mm/y.

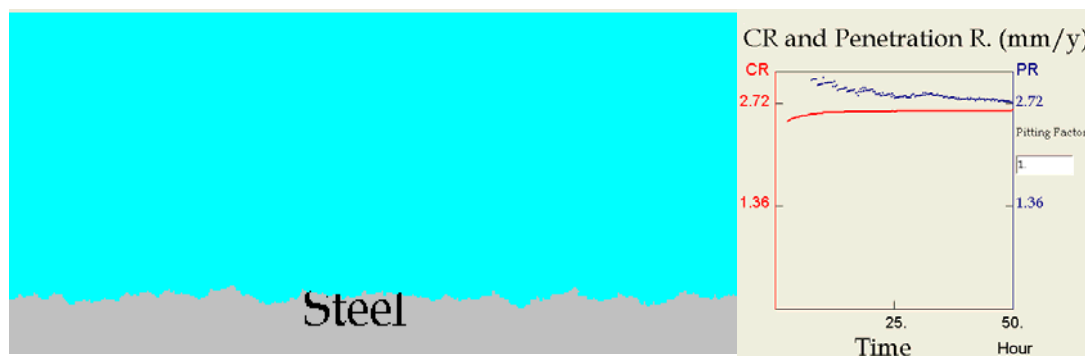


Figure 4.7 Film morphology and corresponding corrosion rate predicted by 2-D model at 0.54bar  $p_{CO_2}$ , 0ppm  $Fe^{2+}$ , 80 °C, pH 6.6, 1m/s

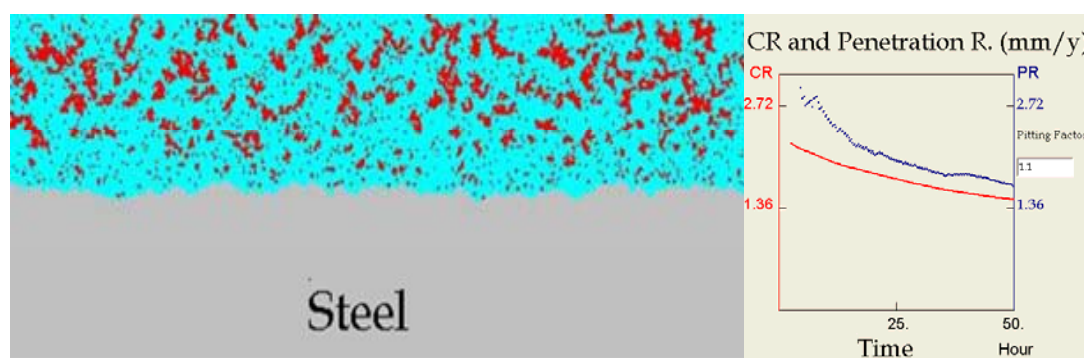


Figure 4.8 Film morphology and corresponding corrosion rate predicted by 2-D model at 0.54bar  $p_{CO_2}$ , 5ppm  $Fe^{2+}$ , 80 °C, pH 6.6, 1m/s

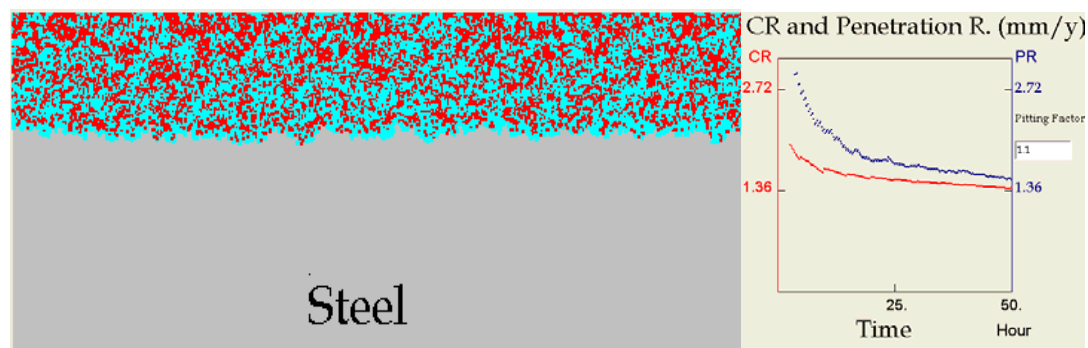


Figure 4.9 Film morphology and corresponding corrosion rate predicted by 2-D model at 0.54bar  $p_{CO_2}$ , 10ppm  $Fe^{2+}$ , 80 °C, pH 6.6, 1m/s

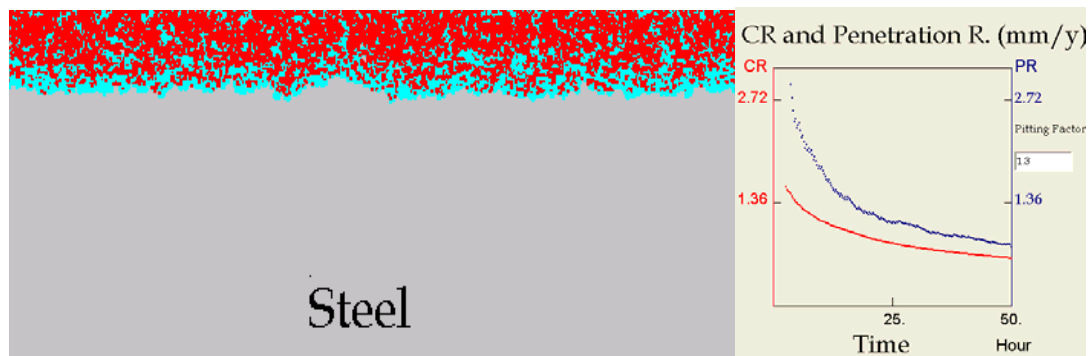


Figure 4.10 Film morphology and corresponding corrosion rate predicted by 2-D model at 0.54bar  $p_{CO_2}$ , 25ppm  $Fe^{2+}$ , 80 °C, pH 6.6, 1m/s



Figure 4.11 Film morphology and corresponding corrosion rate predicted by 2-D model at 0.54bar  $p_{CO_2}$ , 28ppm  $Fe^{2+}$ , 80 °C, pH 6.6, 1m/s



Figure 4.12 Film morphology and corresponding corrosion rate predicted by 2-D model at 0.54bar  $p_{CO_2}$ , 30ppm  $Fe^{2+}$ , 80 °C, pH 6.6, 1m/s



Figure 4.13 Film morphology and corresponding corrosion rate predicted by 2-D model at 0.54bar  $p_{CO_2}$ , 50ppm  $Fe^{2+}$ , 80 °C, pH 6.6, 1m/s

## CHAPTER 5

### CONCLUSIONS

The original two-dimensional (2-D) stochastic algorithm by van Hunnik and Pots [1996] was modified to enable a simulation of localized corrosion morphologies found in practice. The added film formation algorithm and nucleation algorithm predict more realistic film morphology and uniform corrosion rate. The added path searching algorithm improves the quality of prediction.

The original Pots [1996] algorithm, which uses scaling tendency as the only input parameter, was connected with the mechanistic model of Nešić [2003], so that localized attack could be predicted as a function of primitive parameters such as temperature, pH, partial pressure of CO<sub>2</sub>, velocity.

The 2-D model has been successfully calibrated at different film precipitation conditions. Based on the results of the simulations, it was postulated that partially protective films are all that is needed to trigger a localized attack, which is in agreement with the experimental study of Sun [2003].

## CHAPTER 6

## FUTURE WORK

The 2-D model has been carefully calibrated at low pressure (up to 2bar), high temperature (up to 80°C) and various pH values. More experimental data (especially at high pressure) needs to be obtained, so that the likelihood and magnitude of localized attack can be precisely calibrated.

The mechanism behind the model may allow for it to be used in any corrosion/coverage competition condition. Since we know that inhibitor carries out coverage effect to protect the surface from corrosion, and same effect is performed by H<sub>2</sub>S mackinawite. Extending the model under those conditions will extremely improve the utility of the model.

It is suggested to extend the mechanistic 1-D transport/electrochemical model completely into a 2-D model so that localized corrosion can be predicted by using a surface scaling tendency varying with time and depth of the cavity. However, due to the mathematical complexity, the merging of the two models in the presence of passive film is not a simple task.

## REFERENCES

1. Bertocci U., Koike M., S. Leigh, Qiu F., and Yang G., *J. Electrochem. Soc.*, 1986, 133, 1782.
2. Bertocci U., and Huet F., *Corrosion*, 1995, 51, 131.
3. Bowman C.W., “New Developments in the Use of Chemicals for Pipeline Corrosion Control,” *Corrosion Science in the 21<sup>st</sup> Century*, UMIST, 2003.
4. Brossia C.S., and Cragolino G.A., “Effect of Environmental Variables on Localized Corrosion of Carbon Steel,” *Corrosion*, 2000, 56, 5.
5. Bursten, G. T., Pistorius, P.C., and Mattin, S.P., *Corrosion Sci.*, 35, 57 (1993).
6. Cacciuto A, Auer S., and Frenkel D, “Onset of heterogeneous crystal nucleation in colloidal suspensions”, *Nature* 428, 404 – 406, 2004.
7. Calarch Ph., “Theoretical Introduction to Precipitation's Phenomena”, published online: 7 Mar 2001, at <http://www.nano-tek.org/main.html>.
8. Chen J.F., and Bogaerts W.F., “Electrochemical Emission Spectroscopy for Monitoring Uniform and Localized Corrosion,” *Corrosion*, Vol. 52, No. 10, 1996, p. 753.
9. Chokshi K., Board Meeting Report, Sep, 2003.
10. Dabosi F., Beranger G., and Baroux B., *Corrosion Localisee*, les editions de physique, France, 1994, p. 654.

11. de Moraes, F., Shadley, J.R., Chen, J., "Characterization of CO<sub>2</sub> Corrosion Product Scales Related to Environmental Conditions," Corrosion/2000, Paper No.30.
12. de Waard C., Lotz U., and Dugstad A., "Influence of Liquid Flow Velocity on CO<sub>2</sub> Corrosion: A Semi-empirical Model," CORROSION/95, Paper No. 254 (Houston, TX: NACE International, 1995).
13. de Waard, C., Lotz, U., "Prediction of CO<sub>2</sub> Corrosion of Carbon Steel," Corrosion/93, paper no. 69, (NACE international, Houston, TX: 1993).
14. de Waard, C., and Milliams, D.E., " Carbonic Acid Corrosion of Steel," Corrosion, 31, No.5, P.197, 1975.
15. Dugstad, A, Lunde, L., and Videm, K., "Parametric Study of CO<sub>2</sub> Corrosion of Carbon Steel," Corrosion/94, Paper No.14.
16. Dugstad, A., " The Importance of FeCO<sub>3</sub> Supersaturation on the CO<sub>2</sub> Corrosion of Carbon Steels," Corrosion/92, Paper No.14.
17. Fu S., Griffin A.M., Garcia J. G., and Young B., "A New Localized Corrosion Monitoring Technique for the Evaluation of Oilfield Inhibitors," CORROSION/1996, Paper No. 346, NACE International, Houston, Texas, 1996.
18. Gabrielli C., Huet F., Keddam M., and Oltra R., Corrosion, 1990, 46, 266.
19. Gabrielli C., and Keddam, "Review of Applications of Impedance and Noise Analysis to Uniform and Localized Corrosion," M., Corrosion, 1992, 48, 794.

20. Germerdonk K., "Inspection Data Manageet Challenge and Basis of Efficient Risk Management," CORROSION/99, Paper No. 535. (Houston, TX: NACE International, 1999).
21. Gunaltun, Y.M. "Combining Research and Field Data for Corrosion Rate Prediction," CORROSION/96, Paper No. (Houston, TX: NACE International, 1996).
22. Hashimoto M., Miyajima S., and Murata T., Corrosion Science, 1992, 33, 885.
23. Heuer, J.K., Stubbins, J.F., "Microstructure Analysis of Coupons Exposed to Carbon Dioxide Corrosion in Multiphase Flow". Corrosion, 54, No.7, p.566, NACE, 1998.
24. Hoerle S., Sourisseau T., and Baroux B., "Effect of the Electrolyte Composition on the Random/Deterministic Behaviours in Pitting Corrosion," Electrochem. Society Proceedings, Vol. 98, 17, 437.
25. <http://www.corrosion-doctors.org/Localized/Introduction.htm>.
26. Jaycock, N.J., and White, S.P., "A Model for Pit Propagation in Stainless Steels", Electrochemical Society Proceedings, Vol. 98-17, 469.
27. Johnson M. L., and Tomson M. B., "Ferrous Carbonate Precipitation Kinetics and its Impact CO<sub>2</sub> Corrosion," Corrosion/1991, Paper No. 268, NACE International, Houston, Texas, 1991.
28. Jones, D.A, *Principles and Prevention of Corrosion*, 2<sup>nd</sup> edition, Englewood Cliffs, NJ : Prentice Hall ; London : Prentice-Hall International, 1996.

29. Joosten M.W., Johnsen T., Dugstad A., "In Situ Observation of Localized CO<sub>2</sub> Corrosion," CORROSION/94, Paper No. 3.
30. Joosten M.W., Johnsen T., Hardy H. H., Jossang T., and Feder J., "Fractal Behavior of CO<sub>2</sub> Pits", Corrosion/92, Paper No. 11, NACE International, Houston, Texas, 1992.
31. Kaesche, H., "Corrosion of Metals: Physicochemical Principles and Current Problems", Springer, 2003, ISBN 3-540-00626-5.
32. Kermani, M.B., and Smith, L.M., "A Working Party Report on 'CO<sub>2</sub> Corrosion Control in Oil and Gas Production' Design Considerations", European Federation of Corrosion Publication, No.23, The Institute of Materials, 1997.
33. Marsh J., Palmer J.W., and Newman R.C., "Evaluation of Inhibitor Performance for Protection against Localized Corrosion," Corrosion/2002, Paper No. 2288, NACE International, Houston, Texas, 2002.
34. Mullin, J.W., Crystallization, 3<sup>rd</sup> ed. Oxford, U.K.:Oxford Press, 1993.
35. Nescic S., Lee K. J., Corrosion, 2003, 59,616.
36. Nescic S., Nordsveen M., Nyborg R., and Stangeland A., "A Mechanistic Model for Carbon Dioxide Corrosion of Mild Steel in the Presence of Protective Iron Carbonate Films-Part 2: A Numerical Experiment", Corrosion Science, 2003, 59,489.
37. Nescic S., and Lunde L., Corrosion, 1994, 50,717.
38. Nescic S., Postlethwaite J., and Olsen S., Corrosion, 1996, 52,280.

39. Nesic S., Xiao Y., and Pots B.F.M. "A Quasi 2-D localized Corrosion Prediction Model," CORROSION/2004, under review, (Houston, TX: NACE International, 2004).
40. Nordsveen M., Nesic S., Nyborg R., and Stangeland A., "A Mechanistic Model for Carbon Dioxide Corrosion of Mild Steel in the Presence of Protective Iron Carbonate Films-Part 1: Theory and Verification", Corrosion Science, 2003, 59,443.
41. Nyborg R., "Initiation and Growth of Mesa Corrosion Attack during CO<sub>2</sub> Corrosion of Carbon Steel," CORROSION/98, Paper No. 48.
42. Pipeline Performance in Alberta-1980 to 1997, Alberta Energy Utilities Board Report No. 98 – G December 1998.
43. Pistdrius P.C., and Burstein G. T., Philos. Trans. R. Soc. Lond., 1992, A341, 531.
44. Riley, A.M., Wells, D.B., and Williams, D.E., Corrosion Sci., 32, 1307 (1991).
45. Schmitt G., Bosch C., Mueller M., Siegmund G., "A Probabilistic Model for Flow Induced Localized Corrosion," CORROSION/2000, Paper No. 49, NACE International, Houston, Texas, 2000.
46. Schmitt G., Gudde T., and Strobel-Effertz E., "Fracture Mechanical Properties of CO<sub>2</sub> Corrosion Product Scales and their Relation to Localized Corrosion," CORROSION/ 1996, Paper No. 9, NACE International, Houston, Texas, 1996.
47. Stockert L., and Bohni H., Master. Sci. Forum, 1989, 44-45, 313.
48. Sun W., Board Meeting Report, Sep, 2003.

49. Sun Y., Dissertation, Institute of Corrosion and Multiphase Technologies, 2003.
50. Sun Y., Gorge K., and Nesic S., CORROSION/2003, Paper No. 3327, NACE International, Houston, Texas, 2003.
51. Suter, T., Peter. T., and Boehni, H., Mater. Sci. Forum, 192-194, 25 (1995).
52. U. S. Department of Transportation's Research and Special Programs Administration, Office of Pipeline Safety (RSPA/OPS), at [http://primis.rspa.dot.gov/pipelineInfo/stat\\_causes.htm](http://primis.rspa.dot.gov/pipelineInfo/stat_causes.htm), 2004.
53. Uzelac N.I., Willems H.H., and Barbian O.A., "In-line Inspection Tools for Crack Detection in Gas and Liquid Pipelines," CORROSION/98, Paper No. 88, (Houston, TX: NACE International, 1998).
54. van Hunnik E.W.J., and Pots B.F.M., CORROSION/96, Paper No. 6.
55. Williams D. E., Westcott C., and Fleischmann M., J. Electroanal. Chem., 1984, 180, 549.
56. Williams D. E., Westcott C., and Fleischmann M., J. Electrochem. Soc., 1985, 132, 1796.
57. Wu B., Scully J. R., and Hudson J. L., J. Electrochem. Soc., 1997, 144, 1614.
58. Xia Z., Chou K.-C., and Szklarska-Smialowska Z., "Pitting Corrosion of Carbon Steel in CO<sub>2</sub>-Containing NaCl Brine," CORROSION, 1989, 636.